Title
THE STUDY OF MUONIC STATES IN SEMICONDUCTORS

Author
Johnson, Richard Franklin.

Publication Date
1976-11-01

LBL-5526
c. 1

THE STUDY OF MUONIC STATES IN SEMICONDUCTORS

Richard Franklin Johnson
(Ph. D. thesis)

November 1976

Prepared for the U. S. Energy Research and
Development Administration under Contract W-7405-ENG-48

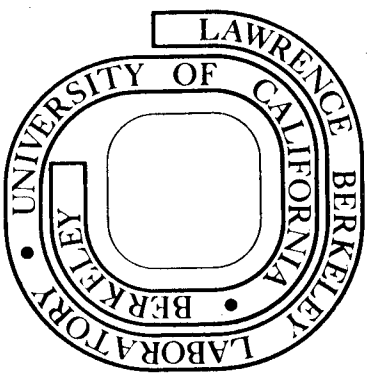

LBL-5526
c. 1

DISCLAIMER

INTRODUCTION

The positive muon (μ^+) has been used for probing the magnetic properties of condensed matter. Because the μ^+ has a magnetic moment, it interacts with the magnetic fields of a sample. Part of the method of using the μ^+ as a magnetic probe involves the production of a beam of μ's whose magnetic moments are longitudinally polarized. The technique of producing a beam will be briefly discussed in Section I, but for the moment we assume that we have a polarized beam of μ's.

The beam of polarized μ's is stopped in a target and each μ^+ until its decay will magnetically behave like a light protron. Each muon will interact with the local magnetic fields of the target. These local fields may arise from hyperfine fields of the electrons or nuclei of the target. When the μ^+ decays, the direction of the μ's magnetic moment is correlated with the direction of its emitted position. Thus, counting decay positrons in a given direction as a function of time spent by the muon in the target gives information about the evolution of the μ's polarization. If a large number of μ's experience the same local magnetic field, the energy of interaction between the magnetic moment of μ and the local field may be observed as a precession frequency. A study of the various precession frequencies observed gives information about what states the μ^+ has formed in the medium.

One state that the μ^+ may form is muonium (Mu) which acts magnetically as a light isotope of hydrogen. Because of the interaction of the μ^+ with its electron in Mu, the μ^+ will precess at a frequency 103 times that of the free μ^+ in an external magnetic field. The factor of 103

arises from the Larmor Precession of triplet muonium where $\omega_{mu} \approx \frac{1}{2} \omega_e = 103\ \omega_u$. A study of the muonium precession frequencies gives information about the electron spin density at the μ^+. This information is directly connected to the dielectric properties of the target.

This dissertation is concerned with the states that the μ^+ forms in semiconductors, in particular, silicon and germanium.

Section I contains the properties of the μ^+ and a brief description of how a polarized μ^+ beam is constructed. A phenomenological description of the slowing down of μ^+ in solids and the possible states formed by the μ^+ is also discussed. The last part of Section I contains a discussion of previous work done with μ^+ in semiconductors.

Section II contains the experimental results of studies done on quartz, silicon, and germanium. Studies were done on the field and temperature dependence of muonium precession frequencies in silicon and germanium. The detection of anomalous frequencies led to a series of experiments that investigated the field and orientational dependence of these frequencies. The muonium and anomalous frequencies were investigated for a series of temperatures between liquid helium temperature and 120°K for p-type silicon.

Section III contains an investigation of several models used to explain the results we have obtained in Si and Ge for muonium precession and the anomalous frequencies.

For muonium precession a brief description is given of the calculation of Wang and Kittel which was done to explain the reduction in the contact interaction for muonium in Si and Ge.

THE STUDY OF MUONIC STATES IN SEMICONDUCTORS

Richard Franklin Johnson

Lawrence Berkeley Laboratory
Department of Physics
University of California
Berkeley, California 94720

ABSTRACT

A beam of polarized positive muons was stopped in semiconducting materials situated in a uniform magnetic field transverse to the beam direction. The precession of the positive muon was observed by detection of the decay positron coming from the asymmetric decay of the muon.

Long-lived muonium was observed via its "two-frequency" precession in p-type samples of silicon and germanium. From the precession frequencies of muonium in silicon and germanium it has been determined that the Fermi contact interaction is reduced in these media compared to its vacuum value. This implies significant screening of the impurity potential of the muon in these materials.

A series of frequencies other than the positive muon and muonium precession frequencies was detected in p-type silicon. The field dependence of these precession frequencies, tentatively designated "anomalous", has been studied for two different crystal orientations in the external field. A shift in these anomalous frequencies has been detected for the two crystal orientations at all fields. Since the states associated with the anomalous frequencies should have symmetries compatible with the lattice structure of silicon which is face centered cubic (diamond structure), a systematic study of magnetic orientational effects was done.

A study of the behavior of the precession frequencies as a function of temperature at 100 G was done for temperature between room temperature and liquid helium temperature. The temperature study indicates a variation of the precession frequencies associated with muonium. At room temperature muonium was not detected.

The formation of muonium is discussed in terms of a deep donor in which the binding energy is greater than half the forbidden gap energy in silicon and germanium.

The formation of the anomalous state is tentatively viewed as a shallow donor state having Tl symmetry. The use of this model leads to the tentative conclusion that the anomalous frequencies may not be associated with shallow donor states.

The apparent variation of the muonium precession frequencies is studied using the model of the formation of a localized moment in which the impurity potential of the muon polarizes the electrons of the valence band. The temperature dependence of this model is investigated to indicate temperature trends in the muonium frequencies.

THE STUDY OF MUONIC STATES IN SEMICONDUCTORS

Contents

Several models are considered in an attempt to explain the anomalous frequencies: (1) excited 2S-muonium, (2) 2P-muonium and (3) shallow donor muonium having Tl symmetry.

The temperature variation of the muonium precession frequencies is investigated via a virtual state model. The temperature trends obtained from the virtual state or "localized moment" moment model point to the possibility of muonium being formed as a virtual state.

I. EXPERIMENTAL PRELIMINARIES

A. μ^+ Properties and Precession Measurements

The positive muon (μ^+) is a particle that has approximately 1/9 the mass of the proton and a charge equal in magnitude to that of the electron. Its mean lifetime is 2.2 μsec, and it decays into a positive electron and two neutrinos. With a spin of 1/2 and a mass a fraction of the proton's mass, the positive muon has a magnetic moment 3.18 times larger than that of the proton; therefore, with consideration for lifetime, mass and magnetic moment, the positive muon can be viewed magnetically as a light proton.

As a result of the asymmetric decay of the positive muon, its decay positron has a higher probability of emerging from the decay along the direction of the spin of the μ^+. This makes the μ^+ a useful probe of magnetic fields in media. The information about magnetic fields can be obtained by observing the time distribution of the decay of a large number of polarized μ's which have stopped and are precessing in a target of interest.

The early experiments[1,2] that used the positive muon as a probe in semiconductors were concerned with the various changes in the μ's polarization. The residual polarization (final μ^+ polarization) was measured for a variety of doping and temperature conditions. A small residual polarization implied that the muon's spin had interacted strongly with target medium, which meant that the muon had formed a complex which lasted long enough to cause its spin to depolarize, due to the μ's interaction with the internal magnetic field of the complex.

B. Polarized μ^+ Beams and Muonic States in Semiconductors

At the 184 Inch Synchrocyclotron at LBL, a 730 MeV proton beam is produced which is used to bombard a copper target for the production of π mesons. The π's have a parity violating decay which results in a positive muon and a neutrino. Because the π's decay in flight, and since the μ has substantial momentum (29 MeV/c) in the center of mass system, one is able to separate the forward and backward spins of the polarized muon beam. In the center of mass system the μ's spin is antiparallel to its momentum. Since the π decays isotropically in the c.m. frame, then the higher energy μ's in the lab frame will tend to have their spins antiparallel to the beam.

The higher energy muons are stopped in a target of interest and begin to precess in an external field transverse to the polarized beam (Fig. 1). The precession of the muons in whatever local fields they experience will be determined by counting the number of decay positrons as a function of time spent by the μ^+ in the target. The angle between the muon spin and the observable positron trajectory will vary in time as $\theta = \omega t$ (see Fig. 2).

The positron rate in the counter telescope as a function of muon lifetime in the target will be given by

$$N(t) = N_0 \exp(-t/\tau_\mu)\left[1 + \sum_i A_i(t)\ \mathrm{Cos}(\omega_i t + \phi_i)\right] + B \qquad (I.1)$$

where the sum is over all possible states the muon can be in, N_0 is the mean number of counts per bin, τ_μ is the mean lifetime of the muon (2.2 sec), ω_i is the precession frequency of the muon in the external magnetic field and whatever local field it experiences, ϕ_i is the initial phase of the muon in the state i, $A_i(t)$ is the muon asymmetry

in state i which may be time dependent in general, and B is the background which was in the experiment at LBL reduced to 1 to 2% of N_o. The parameters in the above equation can be determined by a maximum likelihood fit. The same information can also be obtained by analysis of the Fourier transform of the data which would give all possible precession frequencies due to local magnetic fields.

A stopped muon (Fig. 1) is determined by the logic combination $(B1 + B2) \cdot M \cdot S1 \cdot \overline{S2X}$. For a decay positron signal the logic combination $S2X \cdot E \cdot S2 \cdot S3 \cdot \overline{(B1 + B2 + M)}$ is used. The stopped muon signal starts a clock and creates a gate which lasts about 12 μsec. Any positron signal which occurs during the gate will stop the clock. Therefore, for each observed muon decay one measures the individual lifetime of the decayed muon. Data from an ensemble of muons stopping in the target will then form a time histogram of the precessing muons (Fig. 3).

Care must be taken not to include events that occur when more than one muon is stopped in the target or more than two decay positrons signals occur during the 12 μsec gate. These "Bad" events are rejected by the logic. The complete details of the experiment can be found in Ref. 3.

Typical counting rates of semiconducting targets of sizes 1 in. in diameter and 3 in. long are for the higher energy μ's:

Incident muons	3000/sec
Stopped muons	1500/sec
Detected positrons (good events)	30/sec
"Bad" events	3/sec

The low number of detected positron events is due to the solid angle of the positron telescope (~2% of 4π steradians).

In the experiments on semiconducting materials in which the lifetime and asymmetry of signals were determined for those signals that had relatively small asymmetries or short relaxation times compared to the μ^+ lifetime (e.g., muonium) approximately 30 million events were accumulated to be used in a maximum likelihood fit of the parameters in Eq. (I.1). Those experiments which were concerned with the variation of the precession frequencies represent from 2 to 10 million events; these data were Fourier analyzed. With the Fourier analysis most of the signals were statistically significant after 2 million events had been accumulated (see Section II).

1. Muon Thermalization and Muonium Formation

Upon entering a target the muon has an energy of about 50 MeV and will first lose energy by scattering with electrons until its velocity approaches that of the valence electrons of the target atoms. When the μ has decelerated to the valence electron speeds (~2 to 3 keV) there is a high probability that muonium can be formed. The time it takes the μ^+ to decelerate to these speeds is $\sim 10^{-10}$ sec.[4,5] From energies of several keV until it thermalizes ($\sim 10^{-12}$ to 10^{-11} sec) the μ^+ will successively capture and lose electrons. A quasi-stable bound state of thermalized muonium may exist in the target depending on the dielectric properties of the electrons in the target. If a bound state of muonium is formed in the target, the μ^+ bound in muonium will precess at a mean frequency 103 times faster than that of a free muon.

There are several other states the positive muon may form (Fig. 4):

(1) Diamagnetic compounds in which the muon will precess at a frequency equal to that of the free muon.

(2) The muon may also form radicals with the atoms of the medium, in which case its precession will depend on the hyperfine interaction it experiences.

(3) In addition to being in ground state muonium, there is a possibility that the muon can be in some of the excited states of muonium. These excited states would have a radii that are large in comparison to the size of a unit cell as is shown below and should have symmetries that are in keeping with the symmetry of the lattice.

An estimate of the sizes and energies of impurities can be made if we consider a hydrogenic atom in a semiconductor. Most semiconductors have large static dielectric constants (e.g., $\varepsilon_{Si} = 11.7$) and one would expect the mean radii and energy of an impurity to be affected. For the hydrogenic impurity in a semiconductor the size of the n^{th} excited state will be:

$$a_n = n^2 a_B \frac{m\varepsilon}{m^*} \quad , \tag{I.2}$$

and the energy will be

$$E_n = - E_o/n^2 \, (m^*/m\varepsilon^2) \tag{I.3}$$

where ε is the bulk dielectric constant, m^* is the effective mass of the electron, a_B is the Bohr radius of hydrogen in vacuum (0.528Å), and E_o is 13.58 eV. For a large dielectric constant and a small effective mass the orbits are large (~60Å in Si compared to a lattice constant of 5.43Å) and the binding energy is small (~0.013 eV compared

to the gap energy of 1.21 eV). The binding energy for those impurity states that are formed in the forbidden gap in semiconductors is usually measured from the bottom of the conduction band. Impurity states near the conduction band edge which contribute electrons to the conduction band are called shallow donor states. From the estimate above of the size and binding energy one would expect the excited states of muonium to be shallow donor states. Any shallow donor states of muonium in crystals with the diamond structure would have to have symmetries disignated by the A1 state (s-like), T1 state (p-like), and E state (d-like).[6] The symmetries of these states have been investigated by Kohn and Luttinger.[7]

(4) The muon can also be in short-lived diamagnetic states. These states would be evidenced by a rapid decay of a component of the muon precession signal.

One possible short-lived diamagnetic state can be envisioned by analogy to the H^- ion; however, one should not take this analogy too strictly in the sense that for the H^- ion there are definitely two electrons associated with the atom giving an average electron spin density at the proton of zero. Whereas for Mu^- there will be one electron, but the spin density at the μ^+ will also be zero because of the interaction of the muon's electron with all of the electrons in the band. This spin density would be expected to fluctuate in time, thereby giving a rapidly decaying component of the muon precession. These considerations are based on the model of the muon being in a virtual state in a band.[8-10]

(5) Several diamagnetic or paramagnetic states can be formed if the muon is able to form defects. In silicon and germanium the

"knock on" energy necessary to completely displace a lattice atom is 14 eV and 25 eV respectively; therefore, there could be a situation in which the muon has just enough energy to displace an atom of the lattice and become trapped by the defect. If this happens, there are two possible environments the μ^+ will experience: (a) a defect center in which the covalent bonds of the surrounding atoms are completely satisfied, thereby leading to a diamagnetic environment, (b) a center in which the bonds of the surrounding lattice atoms are not completely satisfied, leading to a possible paramagnetic situation. If it is a paramagnetic environment, the muon will precess at a frequency different from that of the free muon.

As mentioned earlier, the question of whether a stable bound state of thermalized muonium can exist in the target medium depends on the dielectric properties of the electrons. If the density of electrons is of the order of that in a conductor (degenerate gas), then the electrons will tend to screen the μ^+ and interact with each other. Because of the interaction between electrons, the muon will not have any one electron associated with it; hence, one would expect that in good conductors no stable state of muonium can exist. This is exactly the experimental evidence.[2] As the electron density decreases, the mutual interaction between electrons will decrease until an electron concentration is reached where there will be one electron associated with the muon. In this case a bound state of muonium can exist, and one would expect the formation of quasi-stable thermalized muonium in insulators and semiconductors. The above considerations have been verified experimentally.[1,2]

2. Muonium Hamiltonian and "Two Frequency Precession"

It was mentioned earlier in this section that the asymmetry of the μ^+ may have an additional time dependence. One of the major contributions to this time dependence is the formation of muonium and the resultant contact interaction that the muon experiences with its electron. To investitate this behavior, we assume a Hamiltonian of the form

$$H = A\sigma^{\mu} \cdot \sigma^{e} + (h/2)\, \omega^{\mu} \cdot \sigma^{\mu} + (h/2)\, \sigma^{e} \cdot \sigma^{e} \quad , \qquad (I.4)$$

where

$$A = \hbar\omega_o/4 = (2/3)\, g_e \mu_o^e g_\mu \mu_o^\mu |\Psi(0)|^2 \qquad (I.5)$$

is the contact energy, σ^e and σ^μ are the electron and muon Pauli spin operators, and ω^μ and ω^e are the Larmor frequencies of the muon and electron, respectively, which are given by $\hbar\omega_o^\mu = g_\mu \mu_o^\mu B$ and $\hbar\omega^e = g_e \mu_o^e B$. In this case $g_\mu = 2$ and $g_e = +2$ and $\mu_o = eh/2mc$.

The eigenvalues can be determined by using a set of spin functions $(\uparrow_\mu\uparrow_e, \uparrow_\mu\downarrow_e, \downarrow_\mu\uparrow_e, \downarrow_\mu\downarrow_e)$ which give

$$\begin{aligned}
\omega_1 &= \omega_o/4 + \omega_- = E_1/\hbar \\
\omega_2 &= \omega_o/4 + \sqrt{\omega_o^2/4 + \omega_+^2} = E_2/\hbar \\
\omega_3 &= \omega_o/4 - \omega_- = E_3/\hbar \\
\omega_4 &= -\omega_o/4 - \sqrt{\omega_o^2/4 + \omega_+^2} = E_4/\hbar
\end{aligned} \qquad (I.6)$$

where $\omega_\pm = \frac{1}{2}(|\omega^e| \pm |\omega^\mu|)$. The frequencies ω_1, ω_2, ω_3 can be associated with the triplet state of a Breit-Rabi diagram, and ω_4 with the singlet state (Fig. 5).

The energy eigenstates for the above Hamiltonian for the axis of quantization along the magnetic field will be

$$\begin{aligned} |E_1\rangle &= |\uparrow_\mu \uparrow_e\rangle_{\|} \\ |E_2\rangle &= s|\uparrow_\mu \downarrow_e\rangle_{\|} + c|\downarrow_\mu \uparrow_e\rangle_{\|} \\ |E_3\rangle &= |\downarrow_\mu \downarrow_e\rangle_{\|} \\ |E_4\rangle &= c|\uparrow_\mu \downarrow_e\rangle_{\|} - s|\downarrow_\mu \uparrow_e\rangle_{\|} \end{aligned} \qquad \text{(I.7)}$$

where

$$c = \frac{1}{\sqrt{2}}\left(1 + \frac{x}{\sqrt{1 + x^2}}\right) \quad ; \quad s = \frac{1}{\sqrt{2}}\left(1 - \frac{x}{\sqrt{1 + x^2}}\right)$$

with the "natural" specific field $x = |\vec{B}|/B_0$ where $B_0 = 1585$ G.

Experimentally, for most cases, we are unable to detect the hyperfine (contact) frequency $(\omega_1 - \omega_4)$ directly. Because of the time resolution, frequencies above 200 MHz would be undetected; however, the two precession frequencies $\omega_{12} = \omega_1 - \omega_2$ and $\omega_{23} = \omega_2 - \omega_3$ are well within the experimental resolution.

In general how does the μ's polarization depend on muonium formation? This question can best be answered by considering the μ's initial spin polarization as the axis of quantization (field direction arbitrary). If the available electrons in the target are not polarized, then initially half of the muonium ensemble will form in the state $|a_o\rangle = |\uparrow_\mu \uparrow_e\rangle$ and the other half in $|b_o\rangle = |\uparrow_\mu \downarrow_e\rangle$. If we consider the case of the initial polarization of the μ being parallel to the magnetic field then $|a_o\rangle = |\uparrow_\mu \uparrow_e\rangle_{\|} = |E_1\rangle$ which is a stationary state. For the second half of the ensemble $|b_o\rangle = |\uparrow_\mu \downarrow_e\rangle_{\|} = s|E_2\rangle + c|E_4\rangle$.

This state will have a time dependence

$$|b(t)\rangle = se^{-i\omega_2 t}|E\rangle + ce^{-i\omega_4 t}|E_4\rangle$$

or

$$|b(t)\rangle = e^{-i\omega_2 t}\left(s|E_2\rangle + ce^{i\omega_{24} t}|E_4\rangle\right)$$

$$= e^{-i\omega_2 t}\left[(s^2 + c^2 e^{i\omega_{24} t})|\uparrow_\mu\downarrow_e\rangle_{\|}\right. \qquad \text{(I.8)}$$

$$\left. + sc(1 - e^{i\omega_{24} t})|\downarrow_\mu\uparrow_e\rangle\right]$$

where $\omega_{24} = \omega_2 - \omega_4$. Therefore, the state $|b(t)\rangle$ oscillates between the original state $|\uparrow_\mu\downarrow_e\rangle_{\|}$ and the state $|\downarrow_\mu\uparrow_e\rangle_{\|}$ at a frequency ω_{24}. This means that the polarization of the μ^+ oscillates (for $|b(t)\rangle$) between $P_{max} = 1$ and $P_{min} = \dfrac{(x^2 - 1)}{x^2 + 1}$. These relations can be derived from Eqs. (I.7) and (I.8). The polarization for $|a\rangle$ is +1. Thus the net muon polarization oscillates at angular frequency ω_{24} between $x^2/(x^2+1)$ and +1 giving an average polarization as a function of specific field of

$$P_\mu = 1/2 + 1/2\,\frac{x^2}{1 + x^2} \qquad \text{(I.9)}$$

As can be seen, when the field is large $P_\mu \to 1$, which means that at large fields the μ^+ is effectively decoupled from its electron in muonium.

In the process of slowing down, if the μ^+ is able to capture an electron to form quasi-stable muonium, then the time evolution of the μ's spin will be dependent on the muonium precess ion frequencies and the degree of polarization of the captured electron's spin. The

"proper muonium" or the time evolution of the μ's polarization via its "two frequency" precession in muonium was thoroughly investigated by Ivanter and Smilga.[11] The evolution of the μ's spin polarization is obtained from a Hamiltonian of the form:

$$H = H^{Mu} + \hat{V} + \hat{W} \tag{I.10}$$

where H^{Mu} is the muonium Hamiltonian, $\hat{V}$ represents the interaction of the electron in muonium with the lattice and $\hat{W}$ represents the lattice-lattice interaction. A spin density matrix is defined for muonium in terms of the Pauli spin matrices σ_i.

$$\rho = \frac{1}{2} 1 + \vec{P}_\mu \vec{\sigma}_\mu + \vec{P}_e \vec{\sigma}_e + \sum_{i,j=1} \rho_{ij} \sigma^i \sigma_e^j \quad , \tag{I.11}$$

where $\vec{P}_\mu$ is the muon polarization vector components ρ_{10}, ρ_{20}, $\rho_{30}(x,y,z)$ and and $\vec{P}_e$ is the electron polarization vector components ρ_{01}, ρ_{02}, ρ_{03}. The time evolution of ρ is given by

$$\frac{d\rho}{dt} = -\frac{i}{\hbar} [H,\rho] \tag{I.12}$$

which leads to a set of Wangness-Block equations: Following Invanter and Smilga[10] the time dependent terms $\hat{V}$ and $\hat{W}$ can be viewed as relaxation of the electron's spin and may be replaced by a phenomenological parameter 2ν (spin flip frequency) for all pure and mixed electron components. The results are then

$$\begin{aligned}
\dot{\rho}_{il} &= \frac{\omega_o}{2} (\rho_{jo}\varepsilon_{ilj} - \rho_{0k}\varepsilon_{ilk}) + \omega_j^e \rho_{ljk} - \omega_j^\mu \rho_{\beta l}\varepsilon_{ljk} - 2\nu\rho_i \\
\dot{\rho}_{l0} &= \frac{\omega_o}{2} \rho_{ik}\varepsilon_{ljk} - \omega_i^\mu \rho_{k0}\varepsilon_{lik} \\
\dot{\rho}_{0l} &= \frac{\omega_o}{2} \rho_{jk}\varepsilon_{ljk} + \omega_i^e \rho_{0k}\varepsilon_{lik} - 2\nu\rho_{0l}
\end{aligned} \tag{I.13}$$

The above system of equations splits into two irreducible parts, one part involving longitudinal components of $\vec{P}_\mu$ and $\vec{P}_e$ and the other part the transverse components with respect to the external magnetic field. Introducing the complex combination.

$$\rho_\mu = \rho_{10} + i\rho_{20} \ , \ \rho_e = \rho_{01} + i\rho_{02}$$
$$\rho_\mu' = \rho_{31} + i\rho_{32} \ , \ \rho_e' = \rho_{13} + i\rho_{23} \quad . \tag{I.14}$$

ρ_μ represents the polarization of the μ projected on the (x,y) plain (LB). Further introducing

$$\tilde{\rho} = \begin{Bmatrix} \rho_\mu \\ \rho_e \\ \rho_\mu' \\ \rho_e' \end{Bmatrix} \tag{I.15}$$

The transverse subsystem can be written as

$$\frac{d\tilde{\rho}}{dt} = A \cdot \tilde{\rho} \tag{I.16}$$

where

$$A = \begin{Bmatrix} 2i\zeta x & 0 & -i & i \\ 0 & -\left(\frac{4\nu}{\omega_o} + 2ix\right) & i & 0 \\ -1 & i & -\left(\frac{4\nu}{\omega_o} - 2i\zeta x\right) & \\ i & -i & 0 & -\left(\frac{4\nu}{\omega_o} + 2ix\right) \end{Bmatrix} \tag{I.17}$$

The solution of the above set of equations when there is no spin flip frequency ($\nu = 0$) in the X direction (along the beam) is

$$P_\mu(t) = \frac{1}{4}\left\{\left(1 + \frac{\omega_+}{Q}\right)\cos\omega_{12}t + \left(1 - \frac{\omega_+}{Q}\right)\cos\omega_{23}t \right. \qquad \text{(I.18)}$$

$$\left. + \left(1 - \frac{\omega_+}{Q}\right)\cos\omega_{14}t + \left(1 + \frac{\omega_+}{Q}\right)\cos\omega_{23}t\right\} \quad ,$$

where $\omega_\pm$ is as previously defined and

$$Q = \left(\frac{1}{4}\,\omega_o^2 + \omega_+^2\right)^{1/2} \quad ;$$

$$\zeta = \frac{m_e}{m_\mu} \quad .$$

The ω_{ij} are just the Zeeman transition frequencies in muonium. For long times and large fields the terms associated with ω_{14} and ω_{24} will average to zero

$$P_\mu^x(t) = \cos\frac{\omega_{12} - \omega_{23}}{2}\,t + \cos\frac{\omega_{12} + \omega_{23}}{2}\,t(1 + \cos\omega_o t) \quad ; \qquad \text{(I.19)}$$

$$\Omega = \frac{\omega_{12} - \omega_{23}}{2} \quad , \quad \omega_e = \frac{\omega_{12} + \omega_{23}}{2} \quad .$$

When there is mild relaxation due to spin flipping $\left[\nu^2 << \left(\frac{\omega_o}{2}\right)^2 \times 4\right]$ then

$$P_x^\mu(t) \approx \frac{1}{2}\,e^{-t/\tau_3}\left[\left(\cos\Omega_\gamma t + \frac{\Omega\sin\Omega t}{3\tau_3\Omega_\gamma^2}\right)\cos\omega_- t \right.$$

$$\left. + \left(\frac{2\omega + \Omega^2}{\omega_o\Omega_\gamma^2}\right)\sin\Omega_\gamma t\sin\omega_- t\right]$$

where

$$\tau_3 = \frac{2}{3\nu} \quad ,$$

and the beat frequency is also relaxation dependent

$$\Omega_\gamma = \Omega \sqrt{1 - \frac{\nu^2}{4\Omega^2}} \quad .$$

Therefore, in most experiments the observation of muonium precession will be via its two precession frequencies ω_{12} and ω_{23}.

C. Previous Studies of μ^+ in Semiconductors

The earliest study of muons in semiconductors was done by Feher et al.,[1] who studied a number of silicon crystals with different doping in a longitudinal field at various temperatures (Fig. 6). When they looked at the residual muon polarization as a function of doping, they found that at high hole concentrations ($\sim 10^{18}$ Boron atoms/cm^3) the polarization was nearly at maximum and decreased as the hole concentration decreased to the intrinsic stage (10^{10} carriers/cm^3). As the number of free electrons increased, the residual polarization decreased until it reached a minimum at 10^{14} phosphorus atoms/cm^3 and thereafter began to increase to a maximum at a doping of 10^{18} phosphorus atoms/cm^3. The residual polarization was also studied in n-type Ge at room temperature and liquid nitrogen temperature. It was found that the residual polarization at the lower temperature was 1/3 of that at room temperature.

The subsequent interpretation of this strong dependence of the residual polarization on doping was as follows: When the conduction electron concentration is high, the semiconductor has the properties of a conductor, implying that the μ^+ is interacting with the degenerate electron gas and that the μ^+ does not have any one electron associated

with it. This interaction gives a mean electron spin density of zero at the muon. Because the mean electron spin density is zero, the muon's spin is effectively decoupled from any electron's; hence, there is no net Fermi contact interaction. Because the net contact interaction is zero, the muon is less strongly depolarized thereby giving a large residual polarization.

As the conduction electron density decreases, the mean spin density at the μ^+ increases which would be evidenced by an increase in the depolarization and a decrease in the residual polarization. The mechanism for the reduction of muon's polarization would be the formation of muonium (Mu) in which the muon would experience the Fermi contact interaction of its electron.

The increase of the residual polarization with the increase of the hole concentration was less clearly understood.[1] The mechanism suggested was the capture and loss of electrons that were not in equilibrium with the lattice whereby the effective electron spin density at the muon was decreased.

There are two other possible explanations for the increase in the residual polarization: (1) In the region of 10^{18} holes/cm^3 the holes form a gas that is slightly degenerate (overlap of wave functions) implying that the Fermi level will be near the valence band edge. As the acceptor concentration increases the Fermi level will tend to move from the center of the forbidden gap toward the valence band edge.

If we assume that the muonium level is a localized state in the forbidden gap, then when the Fermi level is above the Mu level muonium can be formed. If muonium can be formed and is quasi-stable the μ^+ polarization will be small. Increasing the hole concentration will

make the Fermi level move lower in the gap and eventually pass the Mu level. Once the Mu level is above the Fermi level quasi-stable muonium cannot be formed or, in other words, the muonium atom will be ionized (free μ^+) leading to a large residual polarization of the μ^+.

(2) The other possible explanation is that muonium is not a localized level in the forbidden gap but it is a virtual state in the valence band. Virtual states have been considered by Friedel[12] in explaining the behavior of magnetic impurities in conductors. Anderson[9] and Wolff[10] have done similar calculations to explain the formation of localized moments. The formation of a localized moment (Mu) would depend on the width of the virtual state, its position in the band and its position with respect to the Fermi level and valence band edge. As the Fermi level moves toward the valence band edge the virtual level will tend to become broader. As the width of the level increases, the localized moment (mean electron spin density at the μ^+) will decrease until it is zero implying no muonium formation and a high residual polarization. This model will be explored in Section III.

The series of experiments done by Eisenstein et al.[2] on samples of Si and Ge in a transverse magnetic field for different dopings and various temperatures gave results similar to those reported by Feher et al.[1] for positive muons in longitudinal fields (Table I). In both series of experiments a gated scaling technique was used which effectively yielded the average polarization over 1-4 μsec. Because of the choice of field direction and/or time resolution, neither experiment was able to demonstrate the presence of muonium. Although they were unable to detect any muonium signals, Eisenstein et al.[2]

postulated that the behavior of the residual polarization could be partially explained by the presence of muonium formation. Ivanter and Smilga's[11] thorough theoretical investigation of the depolarization of the muon via its formation of muonium showed that the "proper muonium" mechanism (coherant precession of a large number of Mu atoms) could explain a number of results that had been obtained experimentally.[2] However, the "proper muonium" mechanism could not fully explain the data of Eisenstein et al.[11] For low fields the polarization of the μ deviated from curves based on proper muonium. The implication is that there are other depolarization effects that the muon experiences in semiconductors.

Although the "proper muonium" mechanism explains a major portion of the μ's depolarization behavior in semiconductors there is, at least for silicon, another depolarizing mechanism that should be taken into account. In our experiments at LBL we have detected another set of frequencies in Si besides μ^+ and muonium. These frequencies are associated with a state or states that will contribute to the depolarization of the μ's spin. Hence at present it would be more appropriate to consider a model of "proper muonium plus anomalous state(s)" depolarization.

Andrianov et al.[13] studied the initial asymmetry and relaxation of the μ^+ in intrinsic Ge in the temperature range between 77°K and 360°K and found that the initial asymmetry and relaxation rate increased as the temperature increased (Fig. 7). It was assumed that the muon precession was proportional to $A(t)\cos(\omega t + \phi)$ where $A(t)$ is the time-dependent asymmetry of the muon, and ω and ϕ are the precession frequency and initial phase, respectively. In n-type Ge;

however, it was found that there was virtually no depolarization of the muon asymmetry. Similar effects were found in Si.

Gurevich et al.[14] were able to detect the presence of long-lived interstitial muonium by its "two-frequency precession" in germanium (Fig. 8). From this measurement they were able to determine that the Fermi contact interaction was 0.56 of that in vacuum implying a significant dielectric screening of the μ^+ potential in Ge.

Andrianov et al.[15] were able to fit the proper muonium mechanism model to their longitudinal data (Fig. 9) in silicon (p-type) and obtained $\omega_{Mu} = 0.405\ \omega_o^{vac}$. Hence, in silicon there is significant screening of the μ's potential.

The motivation of the initial experiments at LBL was the direct measurement of the muonium precession frequencies in a transverse field for silicon. These initial experiments not only met with success but indicated a number of other experiments that should be done. These experiments and their results will be discussed in the next section.

II. EXPERIMENTS AND RESULTS

In the experiments at LBL the presence of long-lived interstitial muonium in Si[16,17] has been detected. It was determined in Si that the contact interaction was reduced compared to its value in vacuum, implying that the dielectric screening of the μ^+ is more effective in Si than in Ge. Not only was the presence of muonium detected, but a number of "anomalous" frequencies were also detected. In order to get a better idea of the magnitude of the g-factor (s) associated with the anomalous frequencies, a series of experiments were done for different values of the external magnetic field between 15 G and 4.4 kG. The field variation of the anomalous precession frequencies was done for two separate orientations of the crystal in the external field: (1) The field along the (111) direction and along the (100) direction. It was determined that there was a shift in the anomalous frequencies between the (111) and (100) directions for all fields investigated. Since shifts in precession frequencies cannot be associated with an s-state, it was decided that information about the symmetry of the state (s) associated with the anomalous frequencies could be obtained by looking at the shift in the precession frequencies as a function of the orientation of a 100 G magnetic field in the [110] plan of the crystal. The lifetime of the muonium and the state(s) associated with the anomalous frequencies was also investigated as a function of the temperature. Both the field orientation and temperature dependence studies were cut short because the 184 Inch Synchrocyclotron was shut down; however, interesting trends can be found in both sets of data.

The screening of the μ^+ in muonium for Si and Ge can be attributed to the dielectric properties of these media, and an estimate can be made of the binding energy of Mu in these semiconductors.[18] Nosov and Ykoleva[19] predicted that the dielectric properties of the medium must be considered, and if shallow donor muonium is formed, the contact interaction should be reduced by a factor of $1/[(m/m^*)\ \varepsilon^2]$, where ε is the bulk dielectric constant, and m^* is the isotropic effective mass of the electron. This simple model is not in agreement with experimental data, which suggest that muonium acts as a deep donor. The binding energy of Mu in Si and Ge was estimated by Wang and Kittel[18] using position-dependent dielectric functions, and they were able to show that Mu acts as a deep donor. This will be discussed in Section III.

Although it is known that there are substantial amounts of hydrogen in Ge and Si, no signals due to hydrogen have been detected by any spin resonance experiment or optical techniques;[20] therefore, muonium, which acts magnetically as a light isotope of hydrogen, can give information concerning what happens to hydrogen in these semiconductors. In this section the series of experiments performed at LBL on some insulators and semiconductors and the results of these experiments will be given.

A. Materials and Equipment

1. Samples

Two types of quartz crystals were used for targest in the experiments: natural and fused quartz. The choice of both kinds of quartz was a test of the possible variation of the muonium precession frequencies as a function of environment. The natural quartz sample had the dimensions of 7.62 cm × 10.16 cm × 12.7 cm and the fused quartz was in the form of a cylinder with a diameter of 7.62 cm and height of 10.16 cm.

For the silicon crystals, five sets of single crystals were used. One sample was n-type compensated for 6×10^{13} carriers/cm^3 at room temperature. Three other sets were p-type with 5×10^{12} Boron atoms/cm^3(P_0), 5.3×10^{13} Boron atoms/cm^3(P_1), and 3×10^{14} Boron atoms/cm^3(P_2). These three sets of p-type Si were used to test the variation of the precession frequencies on doping.

Upon detection of the Mu precession frequencies and the anomalous frequencies, a sample of p-type Si with a high concentration of oxygen ($\sim 10^{18}$ oxygen atoms/cm^3) was used to search for a possible effect of this impurity on the precession frequendies and amplitudes, in particular as a test of the anomalous frequencies.

All of the Si crystals were drawn and grown with their [111] axis parallel to the axis of the rods. With the exception of the sample with the high O_2 content, all crystals were zone-refined.

All of the silicon crystals were 2.54 cm in diameter and 10.16 cm long. An experimental target consisted of three rods aligned to present maximum surface area to the muon beam.

The germanium sample was a single crystal of p-type with 7×10^{14} Boron atoms/cm^3 at room temperature. This crystal was in the form of a rod 5.08 cm in diameter and 10.16 cm long.

All of the above samples were run at room temperature and liquid nitrogen temperature. Two of the p-type silicon samples (P_0, P_1) were run at ten field values at 77°K to test for any indication of doping dependence of the precession frequencies. The higher of these p-type samples (P_1) was run at a number of temperatures from room temperature down to liquid helium temperature (4.2°K). This sample (P_1) was also used in a field orientational study at 77°K and 100 G.

2. Refrigerators

For the liquid nitrogen temperature runs a styrofoam dewar with walls 1/2 in. thick was used. Styrofoam was used because only a very few of the muons stop in its walls (about 2% of those stopping in the sample).

For the series of temperature runs between 4.2°K and room temperature, two refrigerators were used: one by Cryomech Inc. and the other by Cryogenics Inc. Both were 10 watt helium refrigerators. For both refrigerators the sample was mounted on the same copper cold finger with the same vacuum jacket which had windows made of copper that were 5 mils thick.

For the liquid helium runs, the University of Tokyo group,[21] which was involved in μ^- studies in solids was kind enough to allow us the use of their cryostat, developed by Ken Nagamine, of that group, which had copper windows 5 mils thick.

3. Magnetic Fields

The magnetic fields were provided by a set of concentric Helmoltz coils and a set of trim coils to remove the stray fields in the vicinity of the targets, including the magnetic field due to the 184 Inch cyclotron magnet. The fields ranged from 15.5 G to 4.4 kG, with the largest field inhomogeneity in a 3 in. cube about the target at any field being 0.02 G. The magnets were stable and were monitored every hour with a drift of 0.01 G every 24 hr period. The fields above 1 kG were monitored with an NMR probe and a feedback loop provided the capability of keeping the field variation to within 0.001 G at all times.

4. Data Analysis

For all of the targets a maximum likelihood fit was done to obtain N_o, B, A, $T_{2\mu}$, ω_μ, ϕ_μ. A knowledge of ω_μ gave a check of the external magnetic field. With N_o and B determined (see Appendix) the data was then Fourier analyzed. Those peaks which gave a signal to noise of 3 or larger were considered significant. Maximum likelihood fits were also done for the anomalous and muonium frequencies in P_0, P_1, and P_2-Si and for muonium in quartz. These fits gave asymmetries, relaxation times, frequencies and phases. For the targets that were run in the refrigerator, the asymmetry of the μ^+ does not have the contribution due to the copper cold finger subtracted out.

B. Targets and Results

1. Quartz

Fused quartz was run at room temperature and liquid nitrogen temperature. There was no evidence of muonium precession at room temperature but the two frequency precession of muonium was detected at liquid nitrogen temperature (Fig. 10). It was determined that for muonium the contact interaction is equal to its value in vacuum. This seems reasonable because quartz has large interstitial cavities and one would expect little or no dielectric screening from the electrons in these cavities. Muon precession was also detected.

The lifetime of muonium was found to be around 500 ns. The results obtained for quartz are in agreement with Gurevich et al.[14]

2. Germanium

In P-type germanium the precession of muonium was partially detected in that the lower of the two precession frequencies was detected. See Table II and Fig. 11. The lack of the upper precession frequency (less than or equal to the noise) could be attributed to the sample being polycrystalline in nature thereby giving a short Mu lifetime due to surface effects, or, incorrect determination of the impurities in the sample. The germanium sample was the only crystal commercially grown. It is also possible that the Fourier analysis was in error; however, this seems unlikely since 6 million events were analyzed. The signals for Mu were statistically significant (singal/noise > 3) for 2 million events in all samples investigated. The Fourier analysis was tried for several windows, time widths, and starting times with the same lack of an upper Mu

signal. The lower detected Mu frequency is in agreement with Gurevich et al.[14]

3. N-Type Si

In the experiments on N-type Si at room and liquid nitrogen temperatures, the two-frequency precession of muonium was not detected. The μ^+ precession signal was evident at room and liquid nitrogen temperatures. These results are in keeping with those of Feher et al.[1] and implies that if muonium forms, it has a very short lifetime (Table II).

4. P-Type Si

The P_1-type silicon sample was run at room and liquid nitrogen temperatures. The μ^+ precession signal was evident at room temperature, but there was no evidence of Mu precession. At liquid nitrogen temperature not only was the μ^+ precession detected, but the two-frequency precession of muonium was also evident (Fig. 12) and Table III). These frequencies were assigned to muonium after it was determined that the difference in the precession frequencies was proportional to the square of the magnetic field. The difference is not only proportional to the square of the magnetic field but inversely proportional to $|\Psi(0)|^2$. From Eqs. (I.6) the measured muonium precession frequencies are:

$$\omega_{12} = \omega_1 - \omega_2 = \omega_0/2 - \sqrt{\omega_0^2/4 + \omega_+^2} + \omega_-$$

and

$$\omega_{23} = \omega_2 - \omega_3 = -\omega_0/2 + \sqrt{\omega_0^2/4 + \omega_+^2} + \omega_-$$

Now the difference in these precession frequencies is

$$\Delta = \omega_{23} - \omega_{12} = -\omega_o + 2\sqrt{\omega_o^2/4 + \omega_+^2} \quad .$$

For relatively small fields (~100 G) $\omega_o >> \omega_+$ and

$$\Delta \approx -\omega_o + \omega_o\left[1 + \frac{1}{2}\frac{4\omega_+^2}{\omega_o^2}\right] = \frac{2\omega_+^2}{\omega_o} \propto \frac{B^2}{|\Psi(0)|^2} \quad .$$

Hence, we have a direct way of measuring $|\Psi(0)|^2$. From the "two-frequency of muonium it was determined that

$$\frac{|\Psi(0)|^2_{Si}}{|\Psi(0)|^2_{vac}} = 0.44 \pm 0.02$$

which implies that the apparent size of muonium has increased. As is evident from Fig. 12, other frequencies were detected that are lower than the muonium frequencies, but much larger than the free μ^+ precession frequency. These frequencies have been designated "anomalous" frequencies.

To test the dependence of the precession frequencies on doping, two other silicon samples were used (P_0 and P_2). From Table III it can be seen that all of the precession frequencies agree to within the errors. For the highest doping there are two additional frequencies besides the muonium and anomalous frequencies.

Because the muonium and anomalous precession frequencies were not doping-dependent, a study of the field dependence of the anomalous frequencies in P_1-type Si was done (Table IV, Fig. 13) with the field in the [111] and [100] directions. The evidence from the table

and Fig. 13 indicates that these anomalous frequendies are less strongly field dependent than the muonium frequencies. From Fig. 13 it is apparent that there is a shift in the precession frequencies associated with the anomalous state for the [111] and [100] directions. These data suggested a series of runs at 100 G and 77°K for different orientations of the magnetic field in the (100) plane of the crystal. These data would give additional information about the symmetry of the state(s) associated with the anomalous frequencies as well as determine which frequencies are associated with the same state(s). Unfortunately, this series of experiments was cut short by the shutdown of the 184 Inch Synchrocyclotron at LBL for Physics research and the data for the runs that were completed is listed in Table V and Fig. 14.

The most striking aspect of this data is the increase in the number of precession frequencies as the field direction moves into the [110] direction. The shift in the anomalous precession frequencies and the increase in the number of precession frequencies detected leads to the conclusion that the state(s) associated with the anomalous frequencies cannot have symmetries that are of s-character. If the symmetry were s-like as ground state muonium is then there would be no shift in the precession frequencies. In order for these precession frequencies to shift with field orientation there must be some other angular momentum that the state has other than spin (i.e., orbital angular momentum).

A study was done to investigate the temperature dependence of the muonium and anomalous frequencies (Table VI, Fig. 15). Note that the frequencies associated with muonium show a variation with temperature

that is larger than any experimental errors and tend to increase with increasing temperature. These temperature variations cannot be associated with any drift in the magnetic field. From the maximum likelihood fits of the muon precession frequencies, the maximum drift in the field is such that $\delta B/B = 0.02$, which implies a maximum shift in the muonium precession frequencies due to drift of 3.84 MHz and 4.36 MHz for the lower and upper precession frequencies, respectively. However, it must be mentioned that the upper precession frequency which shows the temperature trend may not be associated with muonium. This will be discussed in Section III.

The frequencies associated with the anomalous state(s) were detectable down to liquid helium temperature. The existence of the anomalous frequencies at 77°K and 4.2°K associated with the lack of any detectable muonium signal at the lower temperature has been corroborated by the Bell Labs group.[22]

An experiment on P_1-type Si at 77°K and 4.4 kG was done to investigate the behavior of the μ^+ precession signal. It was determined that there are at least two components of the free muon precession signal. One component has a relaxation time that is greater than 25 μsec and the other component has a short relaxation time of ~30 nsec. The possibilities of what these components are will be discussed in the next section (III) along with the discussion of several models used to explain the interesting behavior of muonium and the anomalous frequencies.

III. DISCUSSION OF RESULTS AND TENTATIVE MODELS

A. μ^+ and Muonium

Perhaps the most significant data obtained along with the muon precession is the detection of the two-frequency precession of muonium and the implied change in the contact interaction in both silicon and germamium (Tables II and III). Because the μ^+ and the Mu signals do appear, they must represent independent populations of the ensemble of muons stopping in the target. In silicon the sum of the asymmetries for μ^+ and muonium accounts for 2/3 of the initial muon asymmetry, which implies a certain fraction of the muons are depolarized in times much shorter than the time resolution of the experiment or have frequencies outside of the resolution of the experiment. There is evidence of at least two components in the μ^+ precession signal obtained at 4.4 kG and 77°K. The rapid decay of one component of the μ^+ signal occurred in approximately 30 nsec, which implies that some of the μ's are initially in quasi diamagnetic states that rapidly change into some other paramagnetic states.

From the muonium precession data obtained from our experiments (77°K, 100 G) at LBL along with the data of Gurevich et al.,[14] an estimate has been made by Wang and Kittel[16] of the binding energy of Mu in Si and Ge. Two methods were employed to calculate the binding energy: (1) a cavity calculation and (2) use of a position dependent dielectric function $\varepsilon(r)$. The cavity calculation will be discussed briefly.

B. Cavity Calculation

The cavity calculation was done initially by Reiss,[23] who used variational wave functions to explain why hydrogen does not ionize in semiconductors. Kaus[24] did a similar calculation by solving the Hamiltonian in the cavity and outside the cavity, and matching the logarithmic derivative at the boundary.

The salient features of the cavity model are: (1) the nucleus is assumed to be in a cavity in which its electron experiences the unscreened Coulomb potential, and (2) outside of the cavity the electron "sees" the fully screened potential. The potential is chosen so that it is continuous at the boundary of the cavity; however, there will be a discontinuity in the electric field.

For computational convenience the variation in the mass is chosen so that within the cavity the electron has its vacuum mass m_0, which changes at the cavity boundary to its effective mass in the semiconductor m^*.

A further approximation used is that which matches the wave function inside the cavity to the envelope function outside the cavity. Since the Bloch function will be periodic in the lattice, we are only concerned with the behavior of the envelope function which satisfies a Hamiltonian of the same form as the wave function in the cavity.[18]

The Hamiltonian will have the form:

$$\frac{-\hbar^2}{2m_i} \nabla^2 \psi_i - V_i \psi_i = E \psi_i \quad , \tag{III.1}$$

where the potential is chosen to be

$$V_i = \begin{cases} V_1 = \dfrac{e^2}{r} - \dfrac{e^2(1 - 1/\varepsilon_o)}{R} & \text{(inside)} \\ V_2 = \dfrac{e}{\varepsilon_o r} & \text{(outside)} \end{cases} ,$$

and

$$m_i = \begin{cases} m_1 = m_o & \text{(inside)} \\ m_2 = m^* & \text{(outside)} \end{cases} ,$$

where ε_o is the bulk dielectric constant.

The above set of equations were solved and the logarithmic derivatives were matched at the cavity boundary to give an eigenvalue equation for the energy as a function of the cavity radius of the following form:

$$\begin{aligned} &1/2[(k_2/k_1) - 1] \times {}_1F_1[L + 1 - \lambda_1 \; ; \; 2(L + 1) \; ; \; k_1R] \\ &\quad \times U[L + 1 - \lambda_2 \; ; \; 2(L + 1) \; ; \; k_2R] \\ &\quad + [(L + 1 - \lambda_1)/2(L + 1)] \times {}_1F_1[L + 2 - \lambda_1 \; ; \; 2(L + 1) + 1 \; ; \; k_1R] \\ &\quad \times U[L + 1 - \lambda_2 \; ; \; 2(L + 1) \; ; \; k_2R] \\ &\quad + (k_2/k_1)(L + 1 - \lambda_2) \times {}_1F_1[L + 1 - \lambda_1 \; ; \; 2(L + 1) \; ; \; k_1R] \\ &\quad \times U[L + 2 - \lambda_2 \; ; \; 2(L + 1) + 1 \; ; \; k_2R] = 0 \end{aligned} \qquad \text{(III.2)}$$

where

$$k_1^2 = \left(8m_o/\hbar^2\right) |E| + e^2(1 - 1/\varepsilon_o)/R] \quad ,$$

$$k_2^2 = (8m^*/\hbar^2) \; |E|$$

$$\lambda_1 = 2m_o e^2/k_1\hbar^2 \quad ,$$

$$\lambda_2 = 2m^* e^2/\varepsilon_o i_2 \hbar^2 \quad ,$$

and ${}_1F_1$ and U are the normal and logarithmic solutions of the confluent hypergeometric equation. The binding energy is shown in Fig. 15 as a function of cavity radius. The best estimate of the experimental values (contact ratios) is obtained when the electron's vacuum mass is used; binding energies of 0.15 Rys and 0.065 Rys are obtained for muonium in silicon and germanium, respectively.[18] These binding energies are associated with ratios of contact energy in the medium to the vacuum of 0.756 for the hexagonal site in Si and 0.787 in Ge. The ratios are slightly higher for the tetrahedral sites.[25] Wang and Kittel[18] were able to get a better estimate of the binding energy by using position-dependent dielectric functions calculated from the data of Walter and Cohen[26] and Vinsome and Richardon.[27] It can be seen from Table VII that muonium seems to be a deep donor. Notice that the estimated binding energy if measured from the conduction band edge in both Si and Ge would put Mu in the valence band since the band gaps are 1.21 eV (0.089 Rys) and 0.81 eV (0.0596 Rys) in Si and Ge respectively. With this model all excited states were shown to be shallow.[18] The value for the contact ratio in Si is in good agreement with the experimentally determined value (0.44).

C. Anomalous States

From Table III and Fig. 11 it can be seen that in silicon there is a set of frequencies that is lower than the Mu precession frequencies but is much higher than the μ^+ precession frequency. These frequencies have tentatively been designated as "anomalous".

We initially considered several models in an attempt to explain not only muonium procession but these anomalous frequencies as well.[17] The two models given the most consideration were:

(1) The muon was coupled to a system in which it experienced a contact interaction similar to, but smaller than, that of muonium. Therefore, its spin Hamiltonian would have the form as that of Mu:

$$H = A\vec{\sigma}^{\mu} \cdot \vec{\sigma}^{e} + \frac{h}{2}\vec{\omega}^{\mu} \cdot \vec{\sigma}^{\mu} + \frac{h}{2}\vec{\omega}^{e} \cdot \vec{\sigma}^{e} \quad , \qquad \text{(III.3)}$$

where again, as in Section I, the σ's are the Pauli spin operators and the Larmor frequencies are those as defined.

When the above Hamiltonian was fit to the anomalous frequency data, both g_e and $|\Psi(0)|^2$ were allowed to vary. The transitions ω_{12} and ω_{23} in the Breit-Rabi diagram (Fig. 5) were fit to the data for the magnetic field along the [111] direction. The best values were: The [111] direction, $g_e = 13 \pm 3$ and $\omega_o/\omega_o(\text{vac}) = 0.0198 \pm 0.0002$; for the [100] direction, $g_e = 13 \pm 3$ and $\omega_o/\omega_o(\text{vac}) = 0.0205 \pm 0.0003$ (Fig. 17). There were two objections that were raised about the Modified Breit-Rabi model: (a) the g-factor obtained for an electron in an s-state is unphysical, because in an s-state the electron's g-factor should be 2, (b) since the precession frequencies are shifted, a pure s-state cannot produce this shift.

(2) The above objections to the interpretation of the phenomenological model led to consideration of the 2-P state of Mu. This model was considered plausible because an inclusion of the electrons orbital angular momentum and its spin-orbit interaction could explain the large factor obtained and the fitted hyperfine interaction.

A conventional phenomenological description of the anomalous precession frequencies can be given by an "effective spin Hamiltonian" formalism that is often used in ESR work:

$$H = J_e \cdot \underset{\sim}{A} \cdot S_\mu + \mu_o^e \vec{B} \cdot \underset{\sim}{g}_e \cdot \vec{J}_e + \mu_o^\mu g_\mu \vec{S}_\mu \cdot \vec{B}_\mu \qquad \text{(III.4)}$$

Where $\underset{\sim}{A}$ and $\underset{\sim}{g}_e$ are tensors and $\vec{J}_e$ is the effective spin of the electron Assuming in this model that $\underset{\sim}{g}_e$ is a scalar and the minimum anisotropy is along the [111] axis for A, then A has only two independent elements: $A_{33} = A_\parallel$ and $A_{11} = A_{22} = A_\perp$. Further, assuming that $J_e = 1/2$ the best fit becomes:

$$(g_e)_{ij} = \delta_{ij} \times (13 \pm 3) \quad ,$$

$$A_\parallel = (0.0198 \pm 0.0002)\, A_o(\text{vac})$$

and $A_\perp = (1.035 \pm 0.02)\, A_\parallel$. Since this model is phenomenological, any other states or wave function considered to explain the anomalous frequencies must give parameters that are consistent with those parameters obtained from the phenomenological Hamiltonian.

1. T_1 State Calculation

It has been suggested[28] that since there is a need for a model that explains the anisotropy in the precession frequencies without having the unnecessarily large g-value for the electron, consideration

of the Tl, conduction band-state in silicon might prove to be fruitful. It has a set of wave functions that are p-like, and one would expect a shift in the transition frequencies as a function of field orientation. This is the model that will be considered.

The two models which will be considered in an attempt to explain the observed precession frequencies for the excited state of muonium will be the (1) isotropic wave functions for the Tl state and (2) the variational wave functions of Kohn and Luttinger.[7]

It will become apparent that to fit the model to the anomalous precession frequency data, one arives at values for the size of the atom that are at odds with the effective mass approximation and cavity calculation.[7,8,18] All of these calculations were unable to demonstrate an excited deep state for muonium. The size of the atom obtained is comparable to that of Mu calculated by Wang and Kittel.[18]

a. Effective Mass Theory. In the effective mass approximation[7,8] for shallow-donor impurity atoms, the central approximation is that there is little or no interband mixing of wave functions; and the wave functions in a band must satisfy a secular equation of the form:

$$[E_\ell(p) + V(x)]\, F_\ell(x) = eF_\ell(x) \quad , \tag{III.5}$$

where $V(x)$ is the impurity potential, $F_\ell(x)$ is the envelope function for the ℓ^{th}-minimum, and E_ℓ is the energy ellipsoid about the ℓ^{th}-minimum in the band, E is given by

$$E_\ell(k) = \frac{1}{2m_t}\left(k_x^2 + k_y^2\right) + \frac{1}{2m_l}\left(k_z - k_o\right)^2 \tag{III.6}$$

where m_ℓ and m_t are the longitudinal and transverse masses of the electron near the ℓ^{th}-minimum.

If the ellipsoidal energy surfaces are replaced by spherical ones, then $m_\ell = m_t = m^*$, and in the approximation of no intraband mixing for silicon, there will be six equivalent wave functions corresponding to the six conduction band minima along the (100) directions. If the intervalley mixing is considered, then the degeneracy is moved and the six wave functions split with increasing energy into a singlet (A1), triplet (T1), and doublet (E). The singlet wave function tends to build up charge at the origin and has the form

$$\Psi_{A1} \propto e^{-r/a} \cos(k_i x_i) \quad .$$

The wave functions for the T1 state tend to be p-like near the origin and have the form

$$\begin{aligned} \Psi_z &= Ae^{-r/a} \sin(k_o r \cos\theta) \quad , \\ \Psi_z &= Ae^{-r/a} \sin(k_o r \sin\theta\cos\phi) \quad , \\ \Psi_y &= Ae^{-r/a} \sin(k_o r \sin\theta\sin\phi) \quad . \end{aligned} \tag{III.7}$$

And finally the E-state wave functions will have a d-like character near the origin and will be of the form

$$\begin{aligned} \Psi_E^{(1)} &= Be^{-r/a}[\cos(k_o r \cos\theta) - \cos(k_o r \sin\theta\cos\phi)] \quad , \\ \Psi_E^{(2)} &= Be^{-r/a}[\cos(k_o r \cos\theta) - \cos(k_o r \sin\theta\sin\phi)] \quad , \end{aligned} \tag{III.8}$$

where the conduction band minima occur at $k_o = 0.86(2\pi/a_{Si})$,[7] and a is the appropriate Bohr radius for the effective mass approximation. We will be primarily concerned with the wave functions for the Tl state in calculating certain average values.

b. Spin Hamiltonian for Tl State. We assume that the μ^+ is in a muonic atom that has the symmetry of the Tl state in silicon, whose Hamiltonian is given by

$$H = \eta S \cdot L + \mu_e(\delta\langle L_z\rangle + 2S) \cdot B \qquad \text{(III.9)}$$

$$+ \eta' \, \delta I \cdot L + \frac{3(S \cdot r)(I \cdot r)}{r^2} - \frac{eh}{2m_u c} I \cdot B \quad ,$$

where S and $\langle L\rangle$ are, respectively, the spin and orbital angular-momentum operators of the electron, and I is the spin operator for the μ^+. The appropriate set of wave functions will be linear combinations of the Ψ's. The extra parameter δ in the Zeeman term for the electron is (m_e/m_e^*), where m_e is the atomic mass of the electron and m_e^* is its effective mass. Note that the effective mass is only included in the nonlocal (orbital) part of the electron's angular momentum. The spin-orbit constant is given by

$$\Psi = \frac{e^2h^2S}{2m_e^2c^2\varepsilon}\left\langle\frac{1}{r^3}\right\rangle \quad ,$$

where the macroscopic dielectric constant for silicon is $\varepsilon_{si} = 11.7$. The hyperfine constant is defined as

$$\eta' = \varepsilon(m_e/m_\mu)\,\eta = \eta\varepsilon/206.76$$

Some spacial averaging must also be done for the operators in the hyperfine term of the Hamiltonian.

After averaging and for an arbitrary field direction, the Hamiltonian becomes

$$\begin{aligned} H = {} & P_0 \bar{S} \cdot \langle L \rangle + P_1[\delta\langle L_z \rangle + 2S_z] \\ & + P_2[(\delta\langle L^+ \rangle + 2S^+)\, e^{-i\phi} + (\delta\langle L^- \rangle + 2S^-)\, e^{i\phi}] - P_3 I_z \\ & - P_4(I^+ e^{-i\phi} + I^- e^{i\phi}) + P_5 I \cdot \langle L \rangle \\ & + P_6(l_z)[I^+ S^+ e^{-i2\phi} + I^- S^- e^{i2\phi}] + P_7(l_z)[I^+ S^- + I^- S^+] \\ & + P_8(l_z)\, I_z S_z + P_9(l_z)[(I^+ S_z + I_z S^+)\, e^{-i\phi} + (I^- S_z + I_z S^-)\, e^{i\phi}] \end{aligned} \qquad \text{(III.10)}$$

and where the P's are linear combinations of the coefficience in Eq. (III.9).

Spin functions were chosen of the form:

$$|\phi_{2i-1}\rangle = |\chi_i\rangle \uparrow_\mu$$

and

$$|\phi_{2i}\rangle = |\chi_i\rangle \downarrow \qquad i = 1,2, \ldots 6 \quad ,$$

where

$$|\chi_i\rangle = \frac{1}{\sqrt{2}} |\Psi_x \pm i\Psi_y\rangle \quad \text{or} \quad |\chi_i\rangle = |\Psi_z\rangle$$

When the above spin functions are used, a 12 × 12 secular determinant is obtained with the largest elements along the diagonal. The off-diagonal terms for moderate fields (50-500) G) are on the order of 1/20 of the diagonal. A way of getting a picture of the behavior of the eigenvalues of this Hamiltonian is to consider only the fine

structure ($|\chi_i\rangle$'s). When the hyperfine interaction is turned on, there will be a small mixing of the spin functions of different J. These mixings will give rise to small but nonzero transition probabilities between states of different J. The allowed transitions were determined by looking at the matrix elements $\langle\Phi_i|I_x|\Phi_j\rangle$.

2. Comparison with Experiment

A maximum likelihood fit of the above model to the anomalous data for the [111] direction ($\theta = 53°, \phi = \pi/4$) and checked by a rotation into the [100] direction ($\theta = 0, \phi = \pi/2$) with the data obtained for the [100] orientation. The best fit to the data was obtained for $\delta = 5.00$ and $a = 2.01 \pm 0.02$Å. The value of δ obtained, implies an effective mass of $m^* = 0.2\ m_0$.

The transitions that were best fitted to the data were of ($\Delta I = \pm 1, \Delta S = \pm 1$). Even though an agreement with experiment was obtained for this model, the size of the atom obtained is not in keeping with the effective mass approximation. The usual sizes of atoms associated with the effective mass approximation have sizes on the order of 16Å and above. Therefore, the use of m* in the Hamiltonian is not justified. With an atom size of 2Å there will not be complete screening and the wave functions should be more like the vacuum wave functions.

Because a physically reasonable result was not obtained, it was thought that the ignoring of the anisotropy in the mass may have had a significant effect. Hence, the variational wave functions of Kohn and Littinger[7] were used, which are

$$\Psi_x = A\exp\left[\sqrt{\frac{y^2+z^2}{a_1^2}+\frac{x^2}{a_2^2}}\right]\sin k_o x$$

$$\Psi_y = A\exp\left[\sqrt{\frac{x^2+z^w}{a_1^2}+\frac{y^2}{a_2^2}}\right]\sin k_o y \qquad \text{(III.11)}$$

$$\Psi_z = A\exp\left[\sqrt{\frac{x^2+y^2}{a_1^2}+\frac{z^2}{a_2^2}}\right]\sin k_o z$$

The Hamiltonian has the same form as before (Eq. (III.10)), with different average values. By using the above wave functions, a maximum likelihood fit to the anomalous frequency data was done (Figs. 18 and 19) with the results $a_1 = 1.500\text{Å} \pm 0.001\text{Å}$, $a_2 = 1.470 \pm 0.001\text{Å}$, and $\delta = 5.2 \pm 0.01$. Again these values are at odds with the effective mass approximation.

D. Comparison of Models

Table VIII has a listing of models that have been discussed with the fitted parameters for each theory and the ancillary information that can be obtained from the fitted parameters.

The dielectric function model of Wang and Kittel[16] gives a contact ratio that is in very good agreement with the experimental value obtained for silicon. The value of the contact ratio for Ge is ~20% lower than the experimental value. This much lower theoretical contact ratio for Ge may be due to the behavior of $\varepsilon_{Ge}(r)$ for small values of $\underline{r}$ or the $\underline{r}$ dependence of the effective mass cannot be ignored. If the lower theoretical contact ratio is soley due to $\varepsilon(r)$, then it implies that the slope of $\varepsilon(r)$ is too shallow for small values of $\underline{r}$

in Ge. The energy values are slightly larger than the gaps in both Si and Ge. Even if the energy estimates are off by 20%, it is clear that ground state Mu acts as a deep donor in both materials. Since the binding energy puts the Mu level just above the valence band edge or just below it, one would expect some temperature effects on the ground state Mu. If the binding energy puts the Mu level above the valence band edge, there is a possibility that the Mu level may enter the valence band because of the variation of the forbidden gap as a function temperature. If the Mu level enters the valence band, it becomes a virtual state and a description of the state using the models of Anderson[9] and Wolff[10] would be appropriate. Formation of a virtual state in the valence band would lead to a temperature variation of the electron spin density at the μ^+ thereby giving a temperature variation of the Mu precession frequencies.

The dielectric function approach of Wang and Kittel[18] is the only model that has an unambiguous connection between the ground states and all excited states; therefore, the anomalous frequencies models will be compared to this model. Even though there may be an error in the calculated energy for ground state Mu in the dielectric function model, the error is much smaller for the excited states because for larger $\underline{r}$ $\varepsilon(r)$ goes over into the static dielectric constant. Hence, a comparison of the binding energies of the states associated with the models used for the anomalous frequencies to the excited states in the Wang and Kittel model should point to whether the anomalous states are deep or shallow donors.

The phenomenological models (2S, 2P) give the best fit to the anomalous frequencies. However, there were several low frequencies that the models could not fit. The T_1 state fits are poor but give contact ratios that are consistent with the phenomenological models (see the excited state values in Table VIII). The wave functions that are used to calculate the ancillary information for the phenomenological models give information that is unphysical; however, there is an unambiguous connection between the T_1 state and the A_1 states and the binding energy can be calculated from the fitted parameters. Since the contact ratio for the T_1 model is consistent with the phenomenological model, the binding energy calculated using this model should be a fair estimate of the true binding energy for the anomalous state.

As can be seen from Table VIII the contact ratios for the anomalous state model are six times larger than the contact ratio for the excited Mu state of Wang and Kittel and the calculated binding energy (using Tl wave functions) is two orders of magnitude larger than the excited Mu binding energy of Wang and Kittel.[18] The calculated binding energy for the anomalous state models would seem to make the anomalous state a deep donor. If the calculated binding is roughly correct then one would not expect the anomalous state to be an excited state of Muonium but some other deep state formed by the μ^+.

To date there have been no frequencies comparable to the anomalous frequencies detected in Ge. There are at least two explanations: (1) The anomalous frequencies are an excited state of Mu in Si for which the transition probabilities to the ground state Mu are small,

whereas in Ge the transition probabilities to the ground state are much larger thereby quenching the signal associated with the excited states. (2) The anomalous frequencies are the result of the μ^+ forming defects in both media, in which case a comparison of the "knock on" energies for completely moving a host atom are ~25 eV and 14 eV for Ge and Si, respectively. This difference in "knock on: energies could explain the lack of these signals in Ge.

It is possible that a deep donor state with Tl symmetry can be formed when the μ creates a defect and is trapped by it; therefore, we can imagine a situation in which some of the stopping muons create defects and are trapped by them. Some of these muons will be in a paramagnetic environment (unsatisfied bonds of the surrounding host atoms), and will give the precession frequencies associated with the anomalous state. The other trapped muons will find themselves in a diamagnetic environment and will precess at the free μ^+ frequency. However, a certain number of these muons in the diamagnetic environment may capture electrons within 30 nsec of being trapped, thereby explaining the rapid decay of one component of the muon precession signal that was detected at 77°K and 4.4 kG. These conjectures need to be tested by experiment.

E. Orientational Dependence

From the data in Table V it is obvious that as the field changes from the [100] direction, the number of precession frequencies tends to increase, reaching a maximum in the [110] direction. This would seem to be evidence that the axis of symmetry for the state associated with the anomalous frequencies is in the [100] direction. The

prominent frequencies (underlined) tend to shift with field direction; however, the relative intensities of the prominent lines do not vary significantly. This behavior is in keeping with the anomalous state having Tl symmetry. Data for more field directions is necessary in order to tag unambiguously each frequency.

F. Temperature Dependence

Examining the data from Table VI, several things become apparent: (1) The prominent signals associated with the anomalous state are present at all temperatures tested. The lifetime of this state was found to be weakly temperature dependent. This information must be taken into account when possible configurations are considered for the anomalous state. (2) Below 40°K, the Muonium frequencies were not detected, but were present from 55 to 140°K. Special attention must be paid to the frequencies that are labeled as Mu for 120 and 140°K. It is evident that the upper frequency labeled has shifted significantly as was point ed out in Section III.

A point of caution must be made about the upper labeled Mu frequency at 120 and 140°K. This frequency may not be associated with muonium. It could be due to some other state.

1. Diffusive Model

One possibility is that at low temperatures Mu is not diffusing and is either at the tetrahedral or the hexagonal site in Si. In order to reach a different site Mu would have to have enough energy to overcome a potential barrier. The activation energy necessary for hydrogen to change sites has been discussed by Weiser.[25,29] Some data have been obtained for hydrogen diffusing in Si and Ge,[20,31]

but these data are for elevated temperatures. Nor is it clear that muonium or hydrogen would be diffusing at very low temperatures. Tentatively it can be assumed that below 120°K, muonium is not diffusing and may be at either site; for example, let us say at the tetrahedral. As the temperature is raised to 120°K and above, some of the muonium atoms are able to occupy the hexagonal site thereby producing different precession frequencies (see Table VI). Hence, the upper precession frequency associated with muonium in Table VI could be due to Mu at an interstitial site of different symmetry. This possibility cannot be ruled out at present.

If one assumes that the upper frequency in Table VI is associated with muonium, then an intriguing possibility presents itself. If there is a variation in the precession frequencies for muonium, then this implies that the contact interaction is temperature-dependent. Stated more exactly: the electron spin density at the μ^+ in muonium would be temperature-dependent.

2. Energy Shifts and Lifetimes

As can be seen from the calculations of Wang and Kittel,[18] the calculated binding energy for muonium would put the bound state of the muon in the valence band of both Si and Ge, i.e., Mu would be 280 MeV below the valence band edge in Si. The only way this can occur is is that a virtual state or, in magnetic terms, a "localized moment" is formed in the valence band. The width of this state and hence its lifetime would depend on its interaction with the electrons of the band. Being near the band edge, one would expect some temperature dependence of the binding energy and lifetime of the Mu.

In this section we will explore some of the consequences of the formation of a localized moment and its temperature dependence.

To investigate the temperature dependence of the binding energy, the theory of localized moments that uses the techniques of Anderson[9] and Wolff[10] will be considered. This theory has been successfully used to explain magnetic impurities in metals.[32-34] An alternative approach to describing localized moments is to use the scattering theory of Friedel,[12] in which the electrons of the band scatter off the impurity potential with correlation included to form a virtual bound state whose lifetime would be inversely proportional to the width of the state. However, an easier physical insight can be obtained how these virtual states arise, by using Anderson's technique.

The essential feature of the theory of localized moments can be seen by considering the Hamiltonian for a pair of electrons in a band having orthogonal wave functions

$$H = H_o + K_{ab} - \frac{1}{2}(1-4\bar{S}_a \cdot \bar{S}_b)\, J_{ab} \quad , \qquad \text{(III.12)}$$

where H_o is the total kinetic energy and

$$K_{ab} = \int |\Psi_a(1)|^2 |V(1,2)| |\Psi_b(2)|^2 \, d\tau \quad , \qquad \text{(III.13)}$$

is the Coulomb repulsion energy between the electrons, and a and b refer to different orbitals. On the other hand

$$J_{ab} = \int \Psi_a^*(1)\, \Psi_b^*(2)\, V(1,2)\, \Psi_a(2)\, \Psi_b(1)\, d\tau \qquad \text{(III.14)}$$

is the exchange energy, and S_a and S_b are the spins of the electrons. Therefore, $\bar{S}_a \cdot S_b$ is (-3/4) for antiparallel spins and (1/4) for

parallel spins. Since the wave functions for this system must be antisymmetric, states can be constructed as follows:

$$\Psi_A = \chi_A(S_a,S_b)[\Psi_a(1)\,\Psi_b(2) + \Psi_a(2)\,\Psi_b(1)]$$

and

$$\Psi_S = \chi_S(S_a,S_b)[\Psi_a(1)\,\Psi_b(2) - \Psi_a(2)\,\Psi_b(1)] \quad ,$$

where the spin functions are given by χ_A (antiparallel) and χ_S (parallel). It can be seen that for the antisymmetric spin states the exchange contribution is zero:

$$H\Psi_A = H_o + K_{ab}$$

and

$$H\Psi_S = H_o + K_{ab} - J_{ab} \quad .$$

If the electrons are in the same orbital then

$$K_{ab} = J_{ab} = U \quad ,$$

with

$$H\Psi_A = H_o + U$$

and

$$H\Psi_S = H_o \quad .$$

It is apparent that the two states differ by the Coulomb repulsion.

To characterize the behavior of a localized state it is assumed that a bound state at energy -E has been formed with an electron of a particular spin orientation, say spin up. Then the electrons with spins down will experience the Coulomb repulsion shifting the

energy for the spindown state to -E + U. When one now includes a covalent admixture of the localized state wave function with those of the band, there will be a reduction in the number of electrons with spin up: raising the energy of the localized state from -E to -E + δnU and lowering the energy of the state with the opposite spin to -E + (1 - δn) U. Therefore, the larger the admixture, the smaller the difference in the energy levels resulting in a smaller localized moment, until a point is reached where the number of up and down electrons is equal, leading to the disappearance of the localized moment. It must be mentioned here that when there are equal populations of up and down electron spins, one has a situation which is comparable to H^-. Therefore, what might be expected from this model is a case in which μ^+ is in a diamagnetic state and is quickly depolarized because of fluctuations in the spin density. Experimentally, this would be detected as a rapidly decaying component of the μ^+ signal. Such decay has been detected in Si at 77° and 4.4 kG.

Hamiltonian

The Hamiltonian we use is of the form

$$H = \sum_{k,\sigma} \epsilon_k n_{k\sigma} + E(n_+ + n_-) + U n_+ n_- + \sum_{k,\sigma} V_{Sk}(C_k^* C_{S\sigma}^* + C_S^* C_{k\sigma}) \quad , \qquad \text{(III.15)}$$

where ϵ_k is the energy of the electrons in the band of momentum $\underline{k}$, $n_{k\sigma}$ is the number operator for momentum $\underline{k}$ and spin σ, and $C_{k\sigma}$ and $C_{k\sigma}^*$ the destruction and creation operators.

The second term in the Hamiltonian is the unperturbed energy of the impurity atom. It is also assumed that the wave function for the localized state is orthogonal to the Wannier function belonging to the electron states in the band.

The third term in the Hamiltonian is the correlation energy between the localized electrons, where previously U has been defined.

The fourth term is the interaction of the localized state with those states of the band where

$$V_{Sk} = \frac{1}{\sqrt{N}} \int \phi_S^*(r)\, V(r) \sum_n e^{i\bar{k}\cdot\bar{R}_n} A(r - R_n) \quad , \qquad \text{(III.16)}$$

and where $\phi_S(r)$ is the wave function of the localized state and $A(r - \bar{R}_n)$ is the Wannier function centered about R_n.

Anderson[9] was able to solve the above Hamiltonians for the density of spins in the localized state and the modified density of states in the band by using Green's function methods. He obtained, for the density of localized spins

$$\rho_{S\sigma}(\varepsilon) = \frac{1}{\pi} \frac{\Delta}{(\varepsilon - E_\sigma)^2 + \Delta^2} \quad ,$$

where Δ, the width of the state is given by

$$i\Delta = \lim_{S\to 0} \sum_k (V_{Sk})^2 \frac{(E_\sigma - \varepsilon_k) - iS}{(E_\sigma - \varepsilon_k)^2 + S^2} \quad ,$$

and the energy of the localized state is

$$E_S = E_\sigma + \Delta E(E_\sigma) \quad ,$$

with

$$E_\sigma = -E + \langle n_{-\sigma} \rangle U \quad ,$$

and

$$\Delta E(E_\sigma) = P\left\{\sum_k \frac{|V_{Sk}|^2}{E_\sigma - \varepsilon_k}\right\}$$

the shift in this state due to its interaction with the states of the band. This shift can be associated with the rigid-band model shift in which all states of the band are shifted because of the impurity potential.[35]

In order to get the number of electrons with a particular spin orientation we integrate the density over all states in the band:

$$\langle n_+\rangle = \frac{1}{\pi}\int_{-\infty}^{0} \frac{\Delta d\varepsilon}{(\varepsilon - E_\sigma)^2 + \Delta^2}$$

$$\langle n_+\rangle = \frac{1}{\pi}\cot^{-1}\frac{E + \langle n_-\rangle U + \Delta E(E_+)}{\Delta(E_+)} \quad . \tag{III.17}$$

And for spin down

$$\langle n_-\rangle = \frac{1}{\pi}\cot^{-1}\frac{E + \langle n_+\rangle U + \ E(E_-)}{\Delta(E_-)} \quad ,$$

where

$$E_\pm = E + \langle n_\mp\rangle U \quad .$$

These equations must be solved self-consistently, which means a simultaneous solution of both equations. In Fig. 20 is plotted the two equations for $\frac{U}{\Delta} \sim 5$, and it is seen that there are three solutions: two in which there is a localized moment ($n_+ = 1$, $n_- = 0$; $n_+ = 0$, $n_- = 1$) and one in which there is no localized moment ($n_+ = n_- = 0.5$). As the width of the state increases, the localized spin density will decrease

until at $U/\Delta \sim 1$ there is no localized moment (Fig. 21). These ideas will be used to investigate the behavior of muonium in semiconductors.

Before getting into the calculation for Mu in semiconductors some physical arguments about the behavior of the level shift and its widths. As the level gets further into the valence band the admixture of the localized state with the states of the band should increase implying that the state should become less distinguishable from those of the band. This would result in a decrease in the shift in the level the further into the band one went giving a maximum shift at the band edge. On the other hand because of the increase of admixture, the level should broaden the deeper the level is in the band which would result in a decrease in the localized moment. In the band gap the width of the level should be extremely narrow. For semiconductors one would expect the following behavior: since both Si and Ge have band gaps that are temperature dependent one would expect the level for Mu to change in the valence band. As the temperature is increased the gap will decrease and since the binding energy for Mu is measured from the conduction band edge it will move deeper into the valence band thereby giving a variation in the localized moment. Hence, experimentally a variation in the muonium signals as the temperature is increased would be expected.

If either the "localized states" or the diamagnetic states are in the band gap their lifetimes would be dependent on whether they were above or below the Fermi level.

Experimentally what has been determined is that as the temperature is raised above 77°K the frequency of the muonium signals increases until at room temperature muonium is no longer detected. As the temperature is lowered from 77°K, to liquid helium temperature (4.2°K) there is no apparent shift in the muonium precession frequency and the muonium signal was undetected below 55°K. Tentatively, this behavior is interpreted as follows: The muon forms a localized moment with the states of the valence band such that at low temperatures this virtual state has equal contributions from the spin-up electron states and spin-down states. If the localized moment energy level is sufficiently close to the valence band edge, then there is a possibility of perturbing the contribution of spin-up and -down states to the localized moment by varying the temperature. When there are equal populations of spins states contributing to the localized moment, one would expect no localized moment to form, and the distribution of states about this level will be symmetric. When the temperature increases, the states contributing to the localized moment above the level will be affected, thereby leading to unequal contributions of up and down spins. These unequal populations will be evidenced by nonzero localized moment, hence muonium precession.

3. Muonium as a Localized Moment

In order to get some idea of the behavior of muonium, a rough quantitative calculation of the pertinent quantities in the last section will be done. It is assumed that the wave function for the localized state has s-character

$$\phi(r) = \left(\frac{1}{\pi a^3}\right)^{1/2} e^{-r/a} \quad , \tag{III.18}$$

where a is the appropriate size of the atom for a given ionization energy.

For the Wannier functions of the band, we assume a free electron gas, so the functions will have the approximate form:

$$A(r - R_n) = \frac{1}{(\pi^3\Omega)^{1/2}} U(r) \frac{\sin k|\bar{r} - \bar{R}_n|}{k|\bar{r} - \bar{R}_n|} \tag{III.19}$$

$$\approx \frac{1}{(\pi^3\Omega)^{1/2}} \frac{\sin k|\bar{r} - \bar{R}_n|}{k|\bar{r} - \bar{R}_n|}$$

where Ω is the volume of a unit cell and R_n is the position of the n^{th} atom in the lattice. It is tentatively assumed the r dependence of the u's is only significant near the atoms of the lattice. Therefore,

$$V_{Sk} = \int d^3r \phi(r)\, V(r)\, A(r - R_n) \quad .$$

Assuming a potential in the Thomas-Fermi approximation,

$$V(r) = \frac{q^2 e^{-\lambda r}}{r} \quad ,$$

where λ is the screening distance for the electron gas, and is given by

$$\lambda = \left[\frac{4mq^2}{2}\left(\frac{3n_o}{\pi}\right)^{1/3}\right]^{1/2} = \left[\frac{4}{a_b}\left(\frac{3n_o}{\pi}\right)^{1/2}\right]^{1/2} \quad .$$

Instead of the Thomas-Fermi screening distance, one can use the parameters that come out of the calculations for the dielectric functions in semiconductors.[36-39] By using the above potential, then

$$V_{Sk} = \frac{4}{\pi}\left(\frac{1}{a^3\Omega}\right)^{1/2}\left(\frac{q^2}{R}\right)\frac{\sin kR}{k[(1/a + \lambda)^2 + k^2]} \quad , \qquad \text{(III.20)}$$

where R is the distance to the nearest neighbor Si or Ge atoms. There is very strong evidence[17] that the muon stops at interstitial sites, and in lattices that have the diamond structure there are two possible sites:[25] the tetrahedral site (r = 2.35Å) or the hexagonal site (r = 2.25Å). It is obvious that there will be slightly more admixture at the hexagonal site than at the tretrahedral site.

Since we are considering a semiconductor, the mean number of spin up electrons at the muon in the virtual state is given by

$$n_\uparrow = \frac{1}{\pi}\int_{-\infty}^{-E_g(T)} \frac{\Gamma_{vb}(\varepsilon)\, f(\varepsilon)\, d\varepsilon}{(\varepsilon - E_\uparrow)^2 + \Gamma_{vb}^2(\varepsilon)} + \frac{1}{\pi}\int_0^{\infty} \frac{\Gamma_{cb}(\varepsilon)\, f(\varepsilon)\, d\varepsilon}{(\varepsilon - E_\uparrow)^2 + \Gamma_{cb}^2(\varepsilon)} \quad , \qquad \text{(III.21)}$$

where the width of the state Γ depends on the location of the localized moment level and the band in which the integral is being evaluated. A similar form is obtained for $n_\downarrow$. The function $f(\varepsilon)$ is the Fermi number density,

$$f(\varepsilon) = \frac{1}{1 + e^{\beta(t-E_f)}} \quad .$$

The width of the state in the valence and conduction bands will have the form

$$\Gamma = \pi \begin{cases} \langle V_{Sk}^2 \rangle_{c,b} \; \rho_{c,b}(\varepsilon) = \Gamma_{c,b}(\varepsilon) \\ \langle V_{Sk}^2 \rangle_{v,b} \; \rho_{v,b}(\varepsilon) = \Gamma_{v,b}(\varepsilon) \end{cases}$$

where $\langle V_{Sk}^2 \rangle$ is the average of V_{Sk}^2 over the appropriate energy surface and

$$\rho_{c,b}(\varepsilon) = \frac{\Omega}{2\pi^2} \left(\frac{2m}{\hbar^2} \right)^{3/2} \varepsilon^{1/2} \quad ,$$

$$\rho_{v,b}(\varepsilon) = \frac{\Omega}{2\pi^2} \left(\frac{2m}{\hbar^2} \right)^{3/2} [-(E_g(T) + \varepsilon)]^{1/2} \quad .$$

Figures 22 through 25 show the variation of the mean number of spins at the μ^+ and the change in the Mu frequencies for two different Boron concentrations (2×10^{14} B atoms/cm^3, 5×10^{18} B atoms/cm^3) in P-type silicon. The calculations were done with and without a variation of the gap with temperature.[39,40] As can be seen, a significant change occurs only when the variation of the gap with temperature is included. The trends of the muonium precession frequencies calculated here makes the localized moment a possible candidate in the explanation of the shifts in the muonium frequencies. It is obvious, however, that the temperature dependence obtained from the localized moment calculation does not resemble the experimental evidence (Fig. 15). This may be attributed to several things: (1) The choice of Wannier function is not realistic, (2) the Mu level in the valence band was held fixed to the valence band edge when the temperature varied and (3) the screening of the μ^+ was assumed to be independent of temperature. The experimental evidence of the apparent

temperature dependence of the muonium precession frequencies (Fig. 15) raises the question of how these frequencies could behave differently as a function of temperature? Returning to the approximate expression for the precession frequencies in small fields we see that

$$\omega_{12} \approx \omega_- - \frac{\omega_+^2}{\omega_o}$$

and

$$\omega_{23} \approx \omega_- + \frac{\omega_+^2}{\omega_o}$$

where

$$\omega_\pm = 1/2(1 \pm \zeta)\ \omega_e \quad ; \quad \zeta = \frac{m_e}{m_\mu} = 1/206.76$$

and

$$\omega_o = \frac{8}{3\hbar}\ g_e \mu_o^e g_\mu \mu_o^\mu |\Psi(0)|^2$$

If muonium is a localized moment, then there will not only be a variation in the contact interaction but the Zeeman terms will also vary with temperature. With this in mind we redefine the following

$$\omega_\pm = 1/2[n(T) \pm \zeta]\ \omega_e$$

$$\omega_o' = n(T)\ \omega_o$$

where $n(T)$ is the mean number of spin up electrons at the μ^+. The mean number of spins will be less than unity. The muonium precession frequencies then become:

$$\omega_{12} \approx 1/2[n(T) - \zeta]\,\omega_e - \frac{[n(T) + \zeta]^2\,\omega_e^2}{4n(T)\,\omega_o} \quad ,$$

$$\omega_{23} \approx 1/2[n(T) - \zeta]\,\omega_e + \frac{[n(T) + \zeta]^2\,\omega_e^2}{4n(T)\,\omega_o} \quad .$$

No temperature variation of the lower muonium precession frequency leads to the conclusion that if muonium is a localized moment, then ω_o must also vary with temperature. The behavior of the experimental data cannot be explained with just a variation of the mean number of spins. Including the temperature variation of ω_o we obtain for the specialized condition $\Delta\omega_{12} = 0$:

$$\Delta\omega_{23} = 2\Delta n(T)\,\omega_e$$

The variation of ω_o with temperature implies a change in the screening of the μ's impurity potential. This seems plausible since the dielectric function depends on the electron number density which is temperature dependent.[43] The specialized condition on $\Delta\omega_{12}$ seems somewhat restrictive but cannot be ruled out at present. It has been brought to our attention that Gerevich et al.[44] have obtained evidence in germanium of a possible temperature variation of the Mu precession frequencies. These developments point to a need for more experimental data before the question of muonium precession in semiconductors is finally understood.

IV. CONCLUSIONS

There are a number of conclusions that can be reached upon examination of the data from experiments performed at LBL:

(1) Muonium is at least a deep donor, and, if atomic hydrogen can exist in Si, it must also be a deep donor. The same argument holds for muonium in Ge using the data of Gurevich et al.[14]

(2) In addition to muonium formation in Si, there is another state in which the muon experiences a hyperfine interaction smaller than the contact in muonium. This has been designated the anomalous state.

(3) The anomalous state has orientational dependence in an external magnetic field that is in keeping with a state that has Tl symmetry.

(4) The precession frequencies associated with the anomalous state are weakly temperature-dependent, which may rule out the possibility that this state is associated with an excited state of muonium. If it were an excited state of muonium, one would expect an increase in the anomalous signal with respect to the muonium precession frequencies as the temperature is raised. At temperatures above 55°K, there is no obvious change in the relative intensities of muonium and the anomalous frequencies.

Since there is an apparent change in the precession frequencies associated with muonium, there exists the possibility that muonium is not only a deep donor, but is more appropriately described as forming a localized moment in the valence band of silicon and germanium. For this localized state the electron spin-density at the muon will be temperature-dependent, and this is evidenced by a variation in the precession frequencies of muonium.

Another possible explanation for the shift in the muonium frequencies is obtained from a model in which the muonium atom needs an activation energy to diffuse from one interstitial site of a given symmetry to another of a different symmetry. As the temperature is raised, the relative populations of muonium atoms will change at both sites creating two different sets of precession frequencies. The possibility of this model, points to a strong need for more experimental data on the temperature dependence not only in silicon but in germanium as well.

There is evidence that the anomalous state are not a shallow-donor state, but is a deep state as well as muonium. This evidence also points to the possibility of the anomalous state being associated with the formation of defects. If defects are formed, they could only occur for epithermal energies of the muon. Therefore, this state would be independent of, or weakly dependent on, the temperature. The above model is in keeping with the data obtained to date. To date no frequencies comparable to the anomalous frequencies have been detected in Ge, possibly due to the relative energies required to form defects in the two semiconductors. One would expect fewer defects to form in germanium than in silicon because the knock-on energy to create defects in germanium is approximately two times the knock-on energy in silicon. Also, because the conduction band minima in Ge are in the [111] direction as compared to Si, where they are in the [100] direction, it is possible the field direction is a bad choice for Ge ([111]). This should be explored experimentally.

V. FUTURE EXPERIMENTS

Muonium precession has only been investigated in indirect-gap semiconductors (Si, Ge). It would prove instructive to investigate muonium's behavior in a few direct-gap semiconductors. For instance, α-Sn is a direct-gap semiconductor that has a zero gap, and may demonstrate some interesting behavior, such as, allowing muonium to form two states: one in the valence band and one in the conduction band. Each muonium state should give entirely different temperature behavior.

Muonium formation should be investigated in Si and Ge as a function of doping in a transverse field. It is also possible to use a low-momentum muon beam and thin films of Si or Ge with a tunable laser to investigate the behavior of muonium as a function of conduction electron concentration.

The above experiments are only a few of those necessary to help us understand the behavior of muonium and, by implication, hydrogen in semiconductors. The future promises to be very fruitful and enlightening with the use of this rather new tool.

ACKNOWLEDGEMENTS

The leg of the journey I have just completed could not have been completed without the help of a number of people. First, thanks goes to my advisor Ken Crowe who differed with my views vociferously when necessary and made me think clearly about the physics that was going on. Thanks to Professor Charles Kittel for discussions about muonium formation in semiconductors.

Special thanks goes to Professors Alan Portis and Sam Liu who suffered my stumbling questions about Solid State Physics (Portis) and localized moments (Liu).

Thanks also goes to the members of our experimental group Jesse Brewer, Fred Gygax, and Bruce Patterson with whom discussions about physics increased my appreciation of this field.

This thesis would not be possible if there were not people like Leal Kanstein and the 184 Synchrocyclotron crew who were very helpful and cooperative when our experiments were in progress.

And finally, thanks goes to my parents who gave me the love and support to pursue my interest in Physics.

This work was supported by the U. S. Energy Research and Development Administration.

APPENDIX. ERROR ANALYSIS FOR FOURIER TRANSFORM

Experimentally, we assume the expression of the counts/bin is of the form

$$N(t) = N_o e^{-\frac{t}{T_\mu}}\left[1 + Ae^{-\frac{t}{T_2}}\cos(\omega t + \phi)\right] + B$$

What we normally do is a maximum likelihood f.t of the data to obtain values for N_o and B. From these we define a quantity.

$$X_j = \left[\frac{N(t_j) - B}{N_o}\right]\exp(t_j/\tau_\mu) - 1 = A\exp(-t_j/t_2)\cos(\omega t_j + \phi) \quad .$$

The error in X_j will be due to: (1) The fit of N_o and B. This is a correlated error and will effect the contents of each bin in frequency space differently. (2) The statistical fluctuations in N(t), which produces errors in the Fourier transform. These errors will be uncorrelated.

Hence assuming B << N(t) then for the correlated errors

$$(\Delta X_j)^2_{corr} \simeq \left(\frac{N(t_j)}{N_o^2}\right)^2 \exp(2t_j/\tau_\mu)(\Delta N_o)^2 \quad ,$$

or

$$(\Delta X_j)_{corr} = \frac{\Delta N_o}{N_o}$$

for the uncorrelated errors

$$(\Delta X_j)^2_{unc} = \left(\frac{\Delta N(t_j)}{N_o}\right)^2 \exp(2t_j/\tau_\mu) \approx \left(\frac{\sqrt{N_o}}{N_o}\right)^2 \exp(2t_j/\tau_\mu) \quad ,$$

or

$$X_{j\ unc} = \frac{1}{\sqrt{N_o}} \exp[t_j/\tau_\mu]$$

Now the Fourier transform without errors is given by

$$a_k = \frac{1}{2N} \sum_{j=0}^{2N-1} x_j \exp[-1\pi k_j/N]$$

where 2N is the number of time bins of width T_b used in the transform.

After some algebra we got

$$a_k = \frac{A}{4N} e^{i\phi} \frac{1 - e^{i2N\left(\frac{-\omega k}{N} + T_b + i\frac{T_b}{T_2}\right)}}{1 - e^{i\left(\frac{-\pi k}{N} + \omega T_b + i\frac{T_b}{T_2}\right)}} ,$$

$$+ e^{-i\phi} \frac{1 - e^{-i2N\left(\frac{\pi k}{N} + T_b - i\frac{T_b}{T_2}\right)}}{1 - e^{-i\left(\frac{\pi k}{N} + T_b - i\frac{T_b}{T_2}\right)}} .$$

Letting

$$\Delta\nu_o = \frac{1}{2NT_o} \quad ; \quad \alpha = \frac{T_b}{T_2} ,$$

[$\Delta V_o \equiv$ lowest frequency in Fourier space]

$$K = 2Na ,$$

then

$$\frac{\omega}{\Delta\nu_o} = 2\pi(n + \delta) \quad ,$$

where n is an integer and $0 < \delta < 1$. With the above definitions and ignoring the second term in the Fourier transform, which is only significant for small k or $k \sim N$ we get.

$$a_k \approx \frac{A}{4N} e^{i\phi} \frac{1 - e^{-\kappa} e^{i2\pi\delta}}{1 - e^{-\alpha} + i\frac{\pi}{N}(n - k + \delta)} \qquad \{\kappa = 2N\alpha\} \; .$$

and the power is

$$P_k = |a_k|^2 = \frac{A^2}{16N^2} \frac{1 + e^{2\kappa} - 2e^{-\kappa}\cos[2(n - k)\kappa + 2\pi\delta]}{1 + e^{-2\alpha} - 2e^{-\alpha}\cos\frac{\pi}{N}(n - k + \delta)]}$$

The power will be a maximum when $k \approx n$ or

$$P_k^{max} = P_k \approx n = \frac{A^2}{16N^2} \frac{1 + e^{-2\kappa} - 2e^{-\kappa}\cos(2\pi\delta)}{1 + e^{-2\alpha} - 2e^{-\alpha}\cos\frac{\pi\delta}{N}} \; .$$

As can be seen from the expression for the power, the bin in which the maximum power occurs is dependent on the value of δ. Hence the peak associated with the transform of X_j will have a width dependent on δ. This width of the peak is a consequence of the finite Fourier transform, and is present even when $T_2 \to \infty$ (α and $\kappa \to 0$). The absolute maximum power occurs when $\delta \to \infty$ or

$$P_{max} = \frac{A^2}{16N^2} \times \frac{1 + e^{-2\kappa} - 2e^{-\kappa}\cos(2\pi\delta)}{1 + e^{-2\alpha} - 2e^{-\alpha}\cos\frac{\pi\delta}{N}}$$

and

$$P_{max}\ \frac{A^2}{16N^2} \times \frac{4N^2\alpha^2}{\alpha^2} = \frac{A^2}{4} \qquad \{\text{if } \alpha << 1 \ ; \ 2Na << 1\} \ .$$

Because $\underline{\omega}$ is not in general an integral multiple of $\Delta\omega_o$ - $2\pi\Delta\nu_o$, the maximum power is shared by the bins surrounding the $k \approx n$ bin.

We now look for the full width half maximum bins (FWHM). They will occur when

$$P'_k = \frac{1}{2}\, P_k^{max} \ ,$$

or

$$\frac{A^2}{16N^2}\ \frac{1 + e^{-2\kappa} - 2e^{-\kappa}\cos[2(n - k')\ \pi + 2\pi\delta]}{1 + e^{-2\alpha} - 2e^{-\alpha}\cos\left[\frac{(n - k')}{N} + \frac{\pi\delta}{N}\right]}$$

$$= \frac{A^2}{32N^2}\ \frac{1 + e^{-2\kappa} - 2e^{-\kappa}\cos 2\pi\delta}{1 + e^{-2\alpha} - 2e^{-\alpha}\cos\left(\frac{\pi\delta}{N}\right)}$$

Letting $k' = n \pm \ell$, then

$$\frac{1}{(1 - e^{-\alpha})^2 + \frac{\pi^2}{\pi^2}\,(\delta \pm \ell)^2} \approx \frac{1}{2}\,\frac{1}{(1 - e^{-\alpha})^2 + \frac{\pi^2}{\pi^2}\,\delta^2 e^{-\alpha}} \ ,$$

or

$$\ell = \delta + \left[\delta^2 + \frac{N^2}{\pi 2}\, e^{\alpha}(1 - e^{-\alpha})^2\right]^{1/2}$$

and the FWHM is

$$\Gamma = 2\ell = 2\left\{\delta + \left[\delta^2 + \frac{N^2}{\pi 2} e^{\alpha}(1 - e^{-\alpha})^2\right]^{1/2}\right\} \quad .$$

When there is no mismatch ($\delta \to 0$)

$$\Gamma = \frac{2N}{\Gamma} e^{\alpha/2} (1 - e^{-\alpha}) \quad ,$$

$4\alpha << 1$ then

$$\Gamma \approx \frac{2N\alpha}{\pi}$$

Hence the width of the peak in Foruier space is due to the mismatch of $\underline{\omega}$ and the relaxation time of the signal.

We now consider what happens to the position and width of the peak when there is a correlated error in x_j. We obtain the Fourier transform

$$b_k = \frac{1}{2N} \sum_{j=0}^{2N-1} (x_j \pm \Delta x_{j\,corr})\, e^{-i \frac{\pi k}{N} j}$$

$$b_k = a_k \pm \frac{1}{2N}\left(\frac{\Delta N_o}{N_o}\right)$$

where $\beta = \frac{T_b}{\tau\mu}$, and letting $B = \frac{\Delta N_o}{N_o}$, the power becomes

$$P_k = |b_k|^2 = |a_k|^2 + \frac{B^2}{(2N)^2} \pm \frac{B}{N}(a + a^*) \quad .$$

As can be seen the maximum power still occurs at $k \approx n$.

For the uncorrelated errors we calculate the error in the power the following way

$$(\delta P_k)^2 = \frac{1}{2N} \sum_{s=0}^{2N-1} \left(\frac{\delta P_k}{\delta x_s}\right)^2 (\Delta x_s)^2$$

where

$$\frac{\delta P_k}{\delta x_x} = \frac{1}{2N} \left[a_N^* e^{-i \frac{\pi k s}{N}} + a_k e^{\frac{i \pi k s}{N}} \right] ,$$

and

$$(\Delta X_s)^2 = \left(\frac{1}{\sqrt{N_o}}\right)^2 e^{2s\beta}$$

so

$$(\delta P_k)^2_{unc} = \frac{1}{4N^2} \left(\frac{1}{\sqrt{N_o}}\right)^2 \sum_{s=0}^{2N-1} \left[a_k^* e^{-i \frac{\pi k s}{N}} + a_k e^{i \frac{\pi k s}{N}} \right]$$

or

$$\delta P_{k\ unc} = \frac{1}{\sqrt{N N_o}} (1 - e^{4\pi\beta}) \left[\frac{a_k^{*2}}{1 - e^{2\beta} e^{-i2 \frac{\pi k}{N}}} \right.$$

$$\left. + \frac{a_k^2}{1 - e^2 e^{i \frac{2\pi k}{N}}} + \frac{P_k}{1 - e^{2\beta}} \right]$$

This error has the same effect as the correlated error of broadening the peak (see Figure), but not shifting the peaks. Therefore, we combine the two errors in quadrature

$$\delta P = \left[(\delta P_k)^2_{unc} + (\delta P_k)^2_{corr} \right]^{1/2} .$$

REFERENCES

1. G. Feher, R. Prepost, and A. M. Sachs, Phys. Rev. Letters 5, 515 (1960).
2. B. Einsenstein, R. Prepost, and A. M. Sachs, Phys. Rev. 142, 217 (1960).
3. J. F. Hague, J. E. Rothberg, A. Schenck, D. L. Williams, R. W. Williams, K. K. Young, and K. M. Crowe, Phys. Rev. Letters 25, 628 (1970).
4. G. W. Ford and C. J. Mullin, Phys. Rev. 108, 477 (1957).
5. V. W. Hughes, D. W. McColm, K. Ziock and R. Prepost, Phys. Rev. Letters. 5, 63 (1960).
6. J. F. Carnwell, Group Theory and Electron Energy Bands (Wiley Interscience, 1969).
7. W. Kohn and J. M. Luttinger, Phys. Rev. 98, 195 (1958).
8. C. Kittel and A. H. Mitchell, Phys. Rev. 96, 1488 (1954).
9. P. W. Anderson, Phys. Rev. 124, 41 (1961).
10. P. A. Wolff, Phys. Rev. 124, 1030 (1961).
11. I. G. Ivanter and V. P. Smilga, Sov. Phys. JETP 27, 301 (1968).
12. J. Friedel, Nuovo Cimento Suppl. 7, 287 (1958).
13. D. G. Andrianov, G. G. Myasisheheva, Yu. V. Obokov, V. S. Roganov, V. G. Firsov, and V. I. Fistull, Sov. Phys. JETP 29, 643 (1969).
14. I. I. Gurevich, I. G. Ivanter, E. A. Meleshko, B. A. Nikol'skii, V. S. Roganov, V. I. Selivanov, V. P. Smilga, B. V. Sokolov, and V. D. Shestoakov, Soc. Phys. JETP 33, 253 (1971).
15. D. G. Andrianov, E. V. Mincricheva, G. G. Myasisheheva, Yu, V. Obukhov, V. S. Roganov, G. I. Savel'lev, V. G. Firsov, and V. I. Fistul, JETP 31, 1019 (1970).

16. K. M. Corwe, R. F. Johnson, J. H. Brewer, F. N. Gygax, D. G. Fleming, and A. Schenck, Bull. Am. Phys. Soc. 17, 594 (1972).

17. J. H. Brewer, K. M. Crowe, F. N. Gygax, R. F. Johnson, B. D. Patterson, D. G. Fleming, and A. Schenck, Phys. Rev. Lett. 31, 143, 144 (1973).

18. J. Shy-Yih Wang and C. Kittel, Phys. Rev. B 7, 713 (1973).

19. V. G. Nosov and I. V. Yakoleva, Sov. Phys. JETP 16, 1236 (1963).

20. C. D. Jeffries (private communication).

21. T. Yamasaki, K. Nagamine, S. Nagamya, N. Shihida

22. A. T. Fiory (private communication).

23. H. Reiss, J. Chem. Phys. 25, 681 (1956).

24. P. E. Kaus, Phys. Rev. 109, 1944 (1958).

25. K. Weiser, Phys. Rev. 126, 1427 (1962).

26. J. P. Walter and M. L. Cohen, Phys. Rev. B 2, 1821 (1970).

27. P. K. W. Vinsome and D. Richardson, J. Phys. C 4, 2650 (1971).

28. S. Pantelides (private communication).

29. K. Weiser, J. Phys. Chem. Solids 17, 149 (1960).

30. A. Van Wieringing and N. Warmoltz, Physica 22, 849 (1956).

31. R. C. Frank and J. E. Thomas, Jr., J. Phys. Chem. Solids 16, 144 (1960).

32. A. M. Clogston, Phys. Rev. 125, 439 (1962).

33. A. M. Clogston, B. T. Matthias, M. Peter, H. J. Williams, and R. C. Sherwood, Phys. Rev. 125, 541 (1962).

34. P. A. Wolff, P. W. Anderson, A. M. Clogston, B. T. Mathias, M. Peter, W. J. Williams, J. App. Phys. 33, 1173 (1962).

35. C. Kittel, Quantum Theory of Solids (Wiley, NY, 1967).

36. D. R. Penn, Phys. Rev. 128, 2093 (1962).

37. Hiashi Nara, J. Phys. Soc. Japan 20, 778 (1965).

38. C. Srinivasan, Phys. Rev. 178, 1248 (1969).

39. C. L. Pearson and J. Bardeen, Phys. Rev. 75, 865 (1948).

40. F. J. Morin, J. P. Maita, Phys. Rev. 94, 1525 (1954).

41. W. Paul and H. Brooks, Phys. Rev. 94, 1128 (1954).

42. T. Muto and S. Oyama, Prog. Theoret. Phys. (Japan) 5, 833 (1950).

43. J. Lindhard Kgl. Danske Viedenskab, Mat-fys. Medd. 28(8) (1954).

44. I. I. Gurerich, B. A. Nikol-skii, V. I. Selivanov, and B. V. Sokolov, JETP 41, 401 (1976).

Table I. μ^+ residual polarization.*

Simple	Resistivity (cm)	Impurity Atoms/cm^3	Residual Polarization 300°K	77°K	4.2-10°K
Si	0.05	4×10^{18} B atoms	0.90±0.01	0.67±0.08	0.45±0.01
	3000.00	3×10^{12} B atoms	0.52±0.05	0.24±0.03	0.24±0.08
	350.00	4×10^{12} P atoms	0.45±0.08	0.15±0.04	0.19±0.05
	50.00	4×10^{13} P atoms	0.07±0.03	0.10±0.03	0.15±0.03
	0.3	2×10^{16} P atoms	0.09±0.03	0.12±0.03	0.16±0.04
	0.03	3×10^{17} P atoms	0.10±0.05		
	0.01	1.5×10^{18} P atoms	1.00±0.07		
	0.003	1.5×10^{18} P atoms	1.07±0.10	0.92±0.09	0.80±0.10
Ge	---	10^{15} P atoms	0.92±0.03	0.23 0.07	0.18±0.07

*Data of Eisenstein et al.[2]

Table II. Precession frequencies for μ^+ and Mu at 100 G.

Sample	Temp. (°K)	μ^+ Asymmetry	ω_μ (MHz)	$T\mu$ (μ-sec)	Mu Asymmetry	ω_{Mu_1} (MHz)	ω_{Mu_2} (MHz)	Other Freq. (MHz)
Quartz	77°	0.042±0.001	1.355±0.004	12.0	0.072±0.005	134.3±0.6	143.2±0.6	---
P-Ge (Boron $7\times10^{14}/cm^8$)	77°	0.067±0.003	1.350±0.002	25.0	0.083±0.007	131.3±0.8	---	---
P_1-Si (Boron $5.3\times10^{13}/cm^3$)	300°	0.094±0.002	1.348±0.003	25.0	---	---	---	7.96±1.6
N-Si	77°	---	1.349±0.002	30.0	---	---	---	---

Table III. Doping dependence 100 G, 77°K.

Sample	μ^+ Asymmetry	ω_μ (MHz)	T_μ (μ-sec)	Mu Asymmetry	ω_{Mu_1} (MHz)	ω_{Mu_2} (MHz)	$\omega_{anom.}$ (MHz)
P_0-Si (5×10^{12}B/cm^3)	0.0132±0.002	1.428±0.001	<92.0	0.042±0.008	131.1±0.6	151.2±0.6	40.7±0.6 45.7±0.6
P_1-Si (5.3×10^{13}B/cm^3)	0.022±0.002	1.365±0.001	<95.0	0.051±0.006	130.1±0.6	150.7±0.6	41.6±0.6 46.5±0.6
P_2-Si (3×10^{14}B/cm^3)	0.022±0.003	1.372±0.001	<91.0	0.046±0.005	131.2±0.6	150.2±0.6	41.2±0.6 44.2±0.6 47.5±0.6 49.3±0.6

Table IV. Precession frequencies for P_1-Si at 77°K for different fields and directions.

Direction	Field (Gauss)	ω_{Mu_1}	ω_{Mu_2}	Anamalous Frequencies	Other Frequencies
[111]	15.5	---	---	37.9±0.8	---
[111]	30	39.0±0.8*	---	48.9±0.8	127.3±0.8
[111]	52	69.7±1.6	75.3±1.6	40.5±0.8 , 46.5±0.8	308.7±0.8
[111]	153	190.7±1.6	---	41.1±0.8 , 43.9±0.8 , 47.1±0.8 , 49.9±0.8	15.5±0.8
[111]	341	---	---	38.9±0.8** , 48.9±0.8	15.2±0.8
[111]	520	---	---	37.6±0.8	---
[111]	1,074	---	---	29.6±0.8 , 38.2±0.8 , 56.8±0.8	---
[100]	15.5	---	---	---	---
[100]	30	40.7±0.8*	---	8.75±0.8 , 13.7±0.8 , 45.8±0.8	126.7±0.8
[100]	52	72.9±1.6	78.6±1.6	25.5±0.8 , 42.9±0.8 , 48.9±0.8 , 56.9±0.8	---
[100]	101.1	132.5±1.6	---	43.3±0.8 , 48.9±0.8	---
[100]	153	191.3±1.6	---	48.9±0.8	---
[100]	1,074	---	---	31.4±0.8 , 60.5±0.8	101.2±0.8

*At these fields and lower ones the two muonium precession frequencies cannot be resolved.
**These frequencies coincide with the second harmonic of the cyclotron r-f structure.

Table V. Orientation dependence of anomalous frequencies (77°K, 100 G).

Direction	ω(MHz)				
[100]	43.3±0.8(s)*	48.9±0.8(s)			
[111]	41.0±0.8(s)	46.5±0.8(s)			
[111]±15°	23.4±1.6(s)	39.0±1.6(s)	58.9±3.5(w)		
[110]		41.1±1.6(s)		101.5±1.6(w)	191.3±1.6(w)
	3.4±1.6(s)	42.8±1.6(s)	47.1±1.6(s)	105.2±1.6(w)	209.1±1.6(w)

*The frequencies labeled s had a signal/noise >6 and the ones labeled w had a ratio between 3 and 6.

Table VI. Temperature dependence of precession frequencies in P_1-Si at 100 G, [111] direction.

Temp. (°K)	A_μ	ω_μ	T_μ (μ-sec)	A_{Mu}	ω_{Mu_1}	ω_{Mu_2}	Other Frequencies
4.2°	0.172±0.002	1.426±0.001	>6.1	---			46.8±0.8
44	0.146±0.003	1.363±0.001	>23.9	---			31.2±0.8 , 40.7±0.8
55	0.135±0.002	1.376±0.001	>14.8	0.0461*	131.5±0.8	146.6±0.8	31.2±0.8 , 40.8±0.8 , 46.0±1.6 , 52.7±0.8 , 76.4±0.8
77	0.078±0.003	1.392±0.004	>6.74	0.051	132.0±0.8	150.7±0.8	41.6±0.8 , 46.8±0.8 , 78.0±0.8
120	0.138±0.003	1.374±0.002	>15.6	0.058	130.5±2.8	(2) 158.8±1.8	46.8±0.8 , 60.5±1.6 , 74.2±0.8 , 101.5±3.8 , 116.3±1.6 , 183.2±1.6
140	0.140±0.005	1.376±0.003	>13.9	0.056	131.5±0.8	(2) 162.4±0.8	

*These asymmetries are approximate and are obtained from the Fourier Transform.

(2)These frequencies may not be associated with the upper muonium precession frequency.

Table VII. Contact interaction ratios and ionization energies for Mu in Ge and Si.[16]

	$\left[\lvert\Psi(0)\rvert^2/\lvert\Psi(0)\rvert^2_{vac}\right]_H$ *	$\left[\lvert\Psi^-(0)\rvert^2/\lvert\Psi(0)\rvert^2_{vac}\right]_T$ **	$-E_H$	$-E_H$	E_{gap}
Ge	0.453	0.478	0.116 Rys	0.126 Rys	0.0596 Rys
Si	0.426	0.429	0.112 Rys	0.116 Rys	0.0891 Rys

*Tetrahedral site.
**Hexagonal site.

Table VIII. Listing of models used to explain Mu and/or the anomalous state in Si.

	Model	Cavity	$\varepsilon(r)$	PHENOMENOLOGICAL		SYMMETRIZED WAVE FUNCTIONS		
				$2S^{\dagger}$	$2P^{\dagger}$	T_1^{iso}		T_1^{ansio}
	Data Used	R_e=.44	R_e=.44	Anom††	Anom	Anom		Anom
	Fitted Parameters	---	---	R_e=.0198 ±.002 g_e=13±3	R_e=.0198 ±.002 g_e=13±3	$\langle r\rangle$=2.01±.01Å $\delta=\frac{m}{m^*}$=5.0±.001		a_1=1.50±.01Å a_2=1.47±.01Å δ=5.2±.01
GROUND STATE	Contact Radio	.756	.427	1.253	1.253	A_1 STATE	.0377 ±.002	.0828 ±.002
	E_I (Rydbergs)	.15	.112	1.078	1.078		.054 ±.002	.066 ±.003
	$\langle r\rangle$*** (in a_B)	2.95	2.61	.928	.028		3.81 ±.02	2.88 ±.04
EXCITED STATE	Contact Ratio	---	.00294	.0198	.0198	T_1 STATE		
	E_I (Rydbergs)	---	.0042	.269	.269			
	$\langle r\rangle$*** (in a_B)	---	31.4	3.71	3.71		3.81 ±.02	

†These models are phenomenological; it is assumed here that $\psi_{1s}(r)=A\, e^{\frac{-r}{a}}$ (hydrogenic), where a is chosen to give the fitted hyperfine interaction.

*The Mu data was the experimentally determined ratio $R_e=|\psi(0)|^2_{Si}/|\psi(0)|^2_{vac}$.

††The anomalous state data were the observed precession frequencies.

**The use of these wave functions assumes that the A1, T1 and E states differ from each other by at most the valley-orbit interaction (~0.031 eV=.00228 Rys).

***a_B is the Bohr radius.

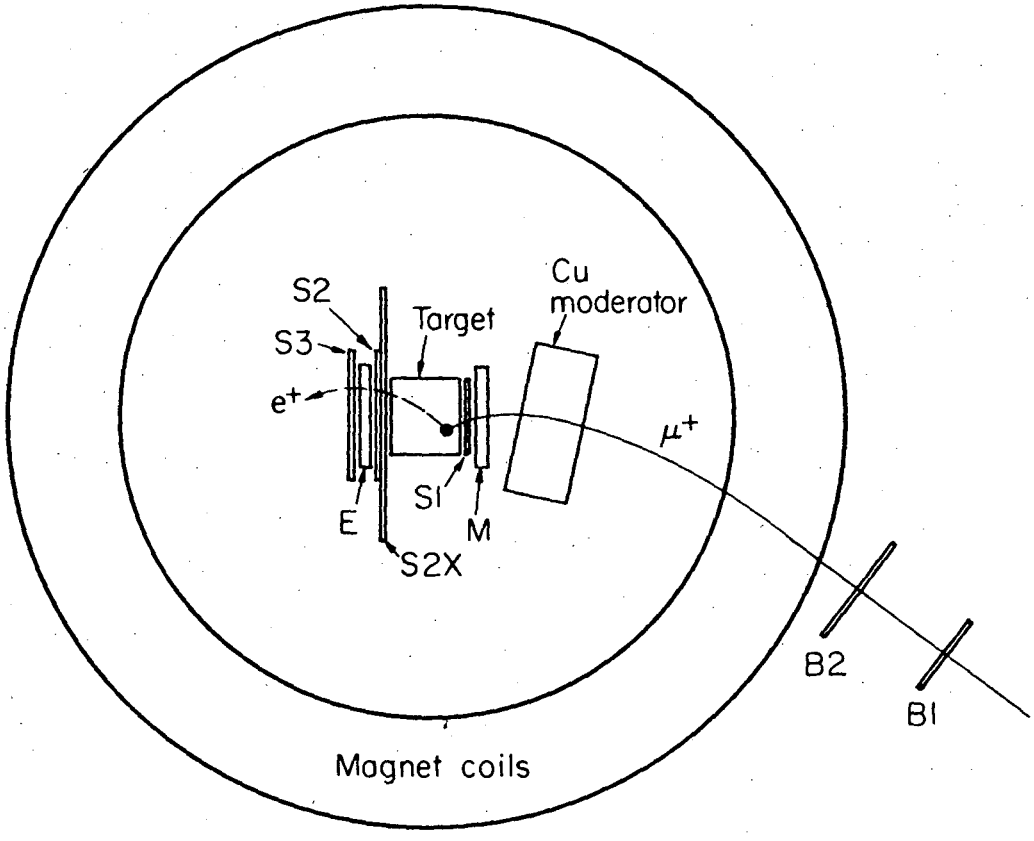

XBL 735-2916A

Fig. 1. Telescope arrangement for detection of muon precession in a transverse external magnetic field.

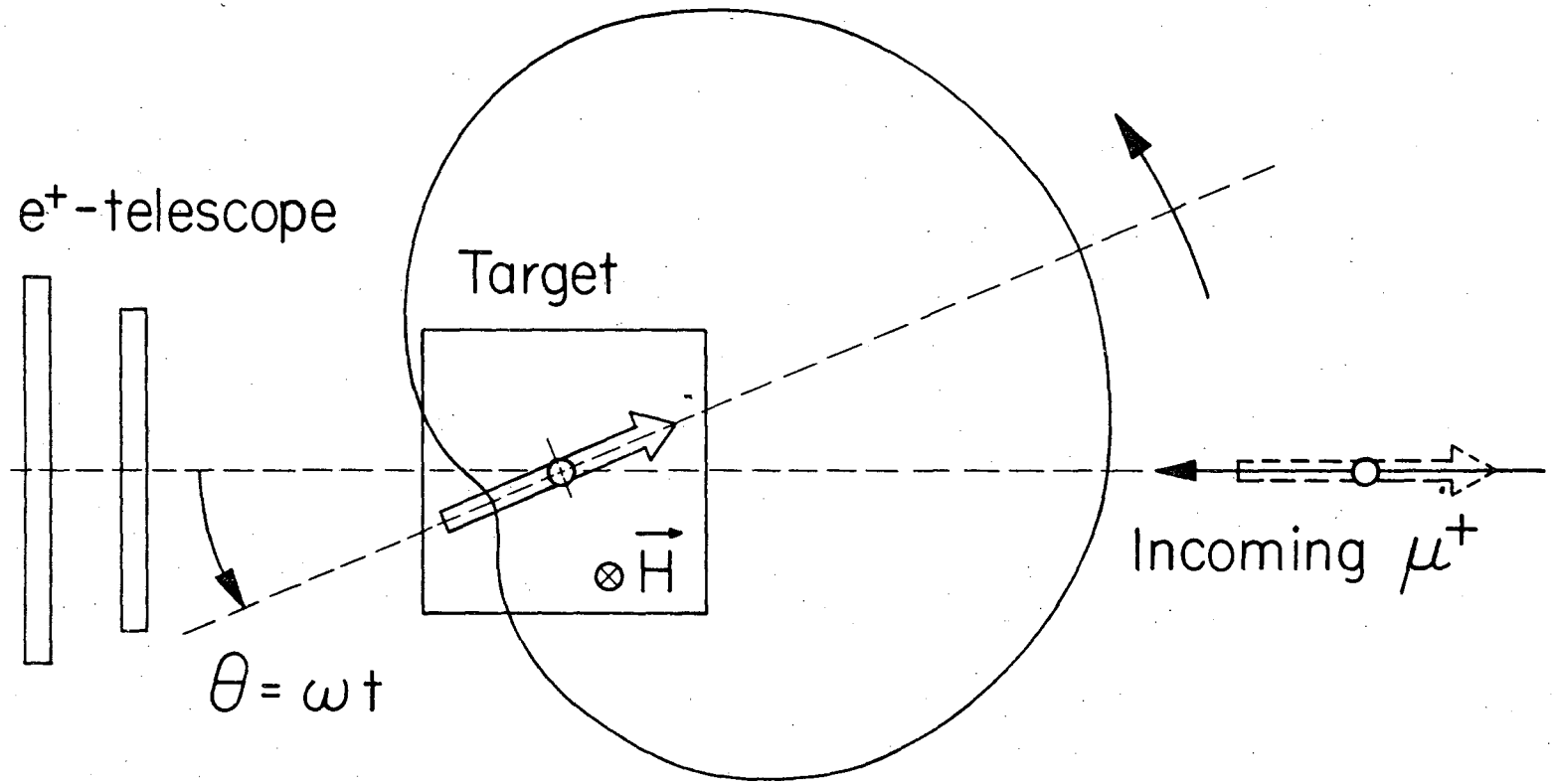

XBL7310-4191

Fig. 2. The relationship between the polarization of the positive muon and its decay electron. The illustration is for higher energy μ's which have their spins (dotted arrow) antiparallel to the beam. The drawn cycloid is the probability distribution of position momenta with respect to the μ's spin direction.

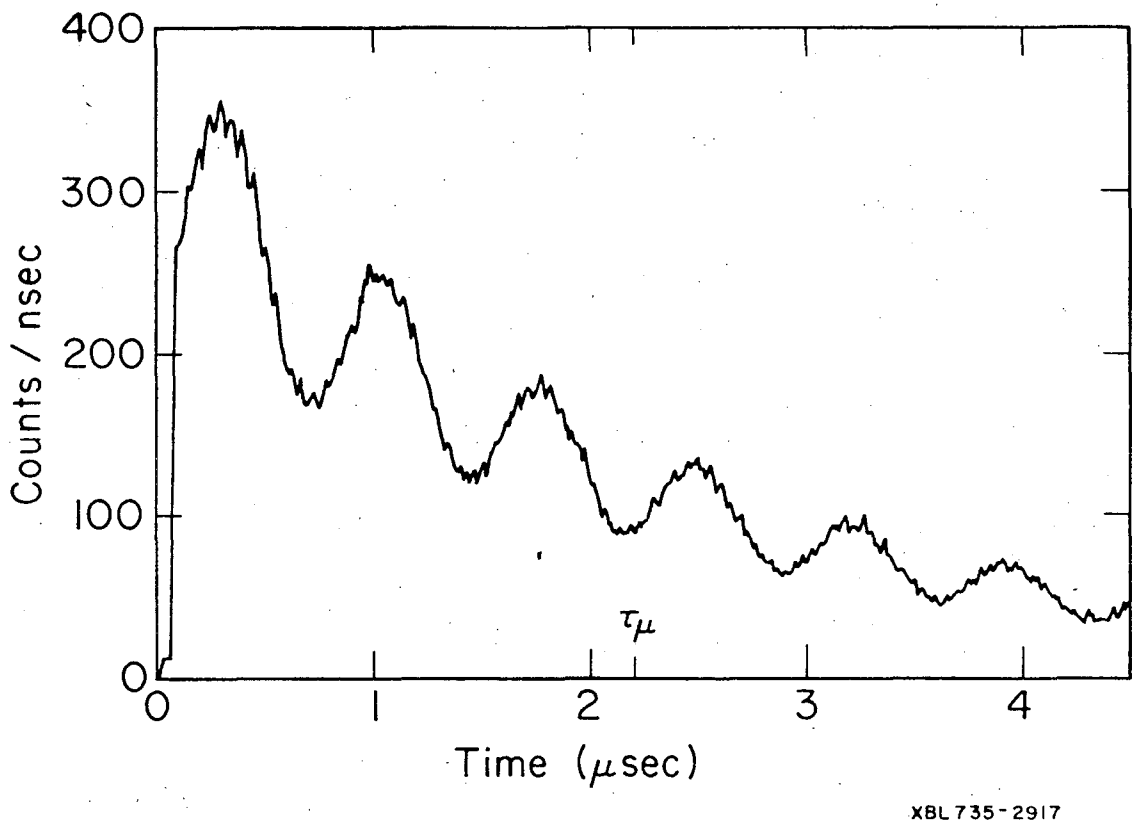

Fig. 3. Time histogram of the precession of the positive muon in carbon tetrachloride. This target gives one of the highest asymmetries for the muon asymmetry implying little or no muonium formation.

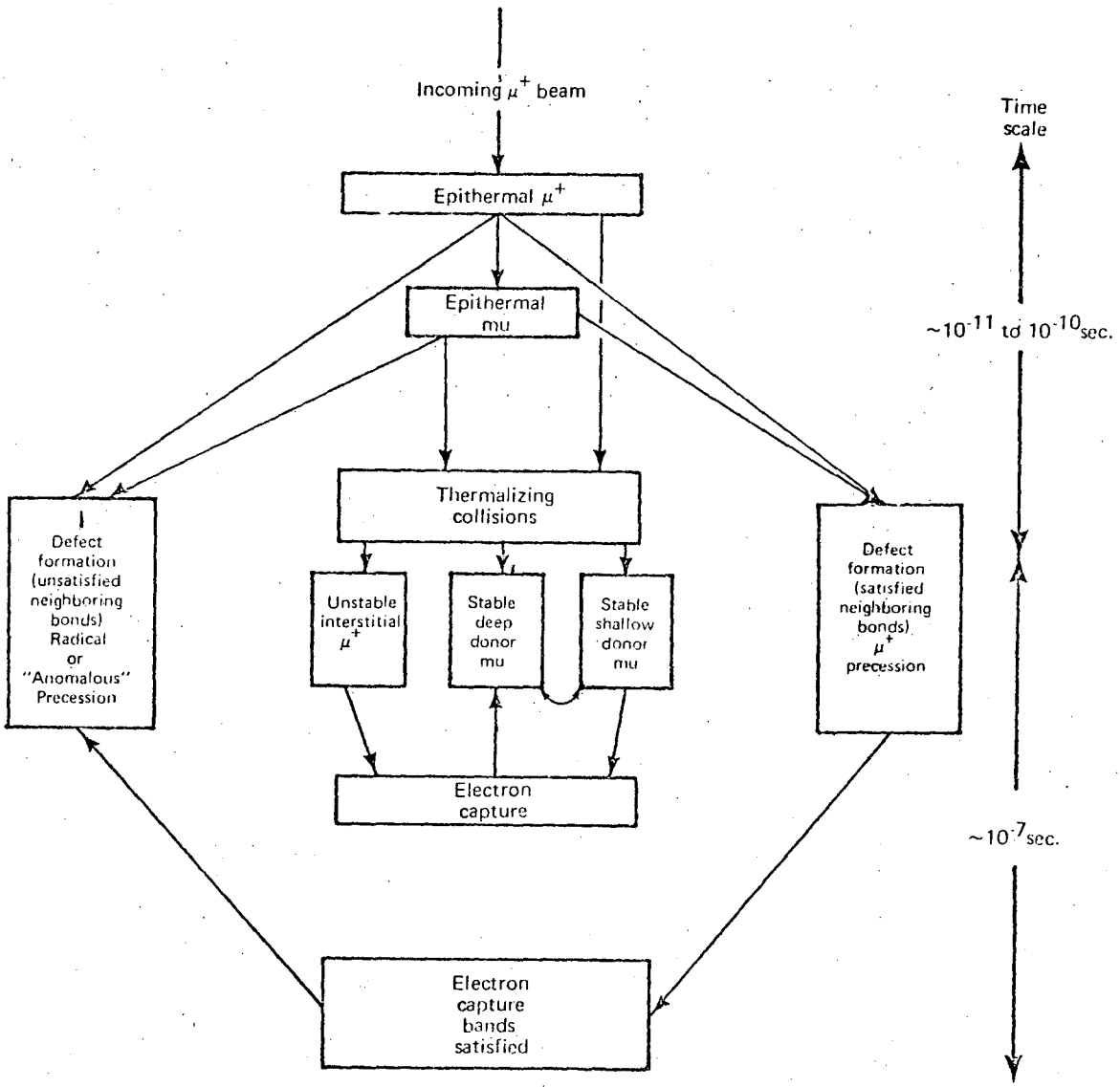

XBL7611-4435

Fig. 4. Schematic representation of possible states formed by the positive muon in semiconductors. There is a wide variety of defects formed by the inelastic collisions of charged particles with host atoms; in this thesis only the simplest defects will be considered. The dotted line connecting deep and shallow Mu allows for possible coherent transitions between these states.

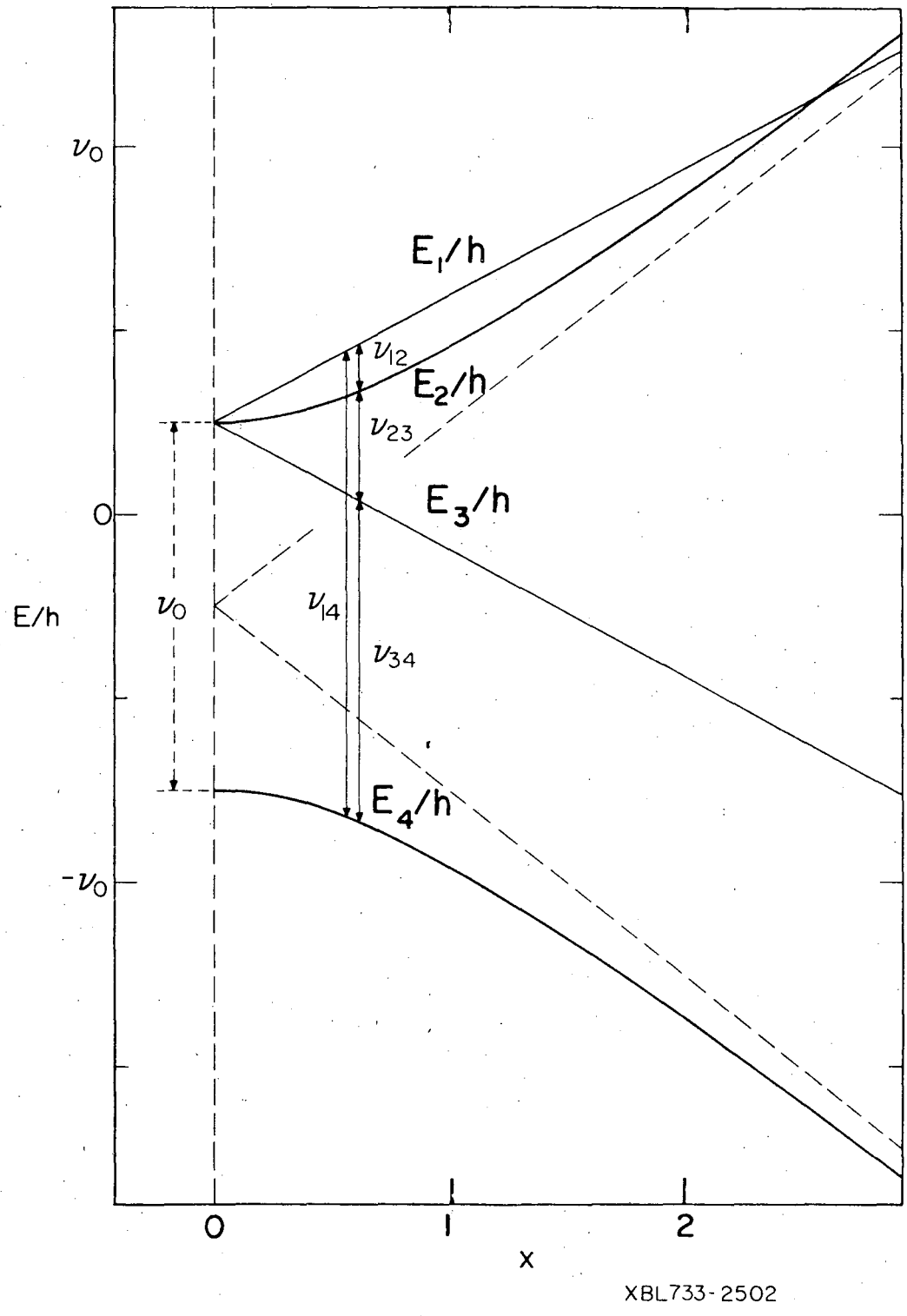

Fig. 5. Energy eigenstates for ground state muonium in an external magnetic field as a function of the dimensionless "specific field" $x = 2\omega_+/\omega_0$ for graphical clarity unphysical values are used for the electron and muon magnetic moments.

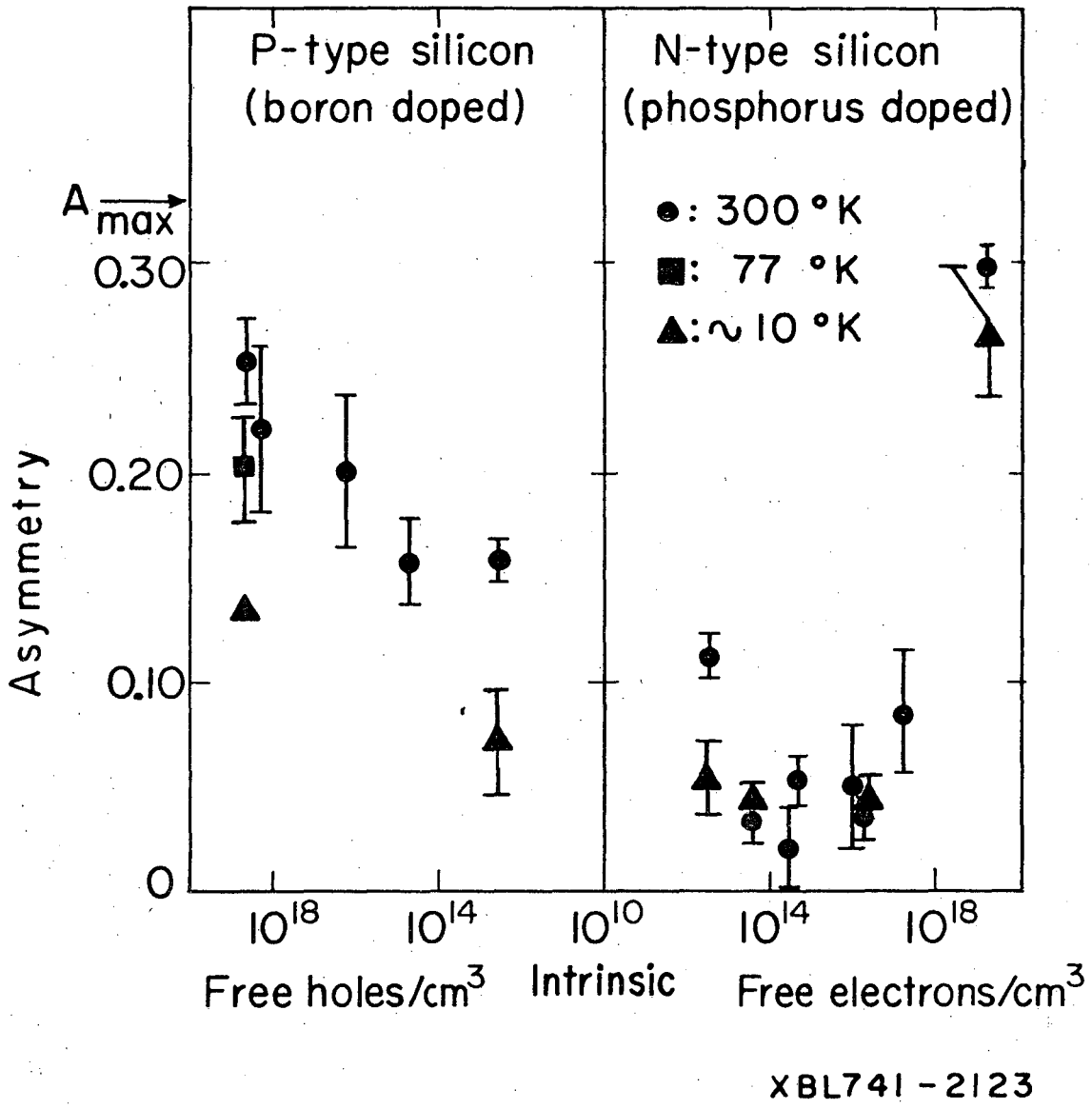

Fig. 6. Experimental values of the positive muon's asymmetry vs the free electron concentration in n-type silicon and free hole concentration in p-type silicon at room temperature, liquid nitrogen temperature and 10°K. Taken from Feher et al.[1]

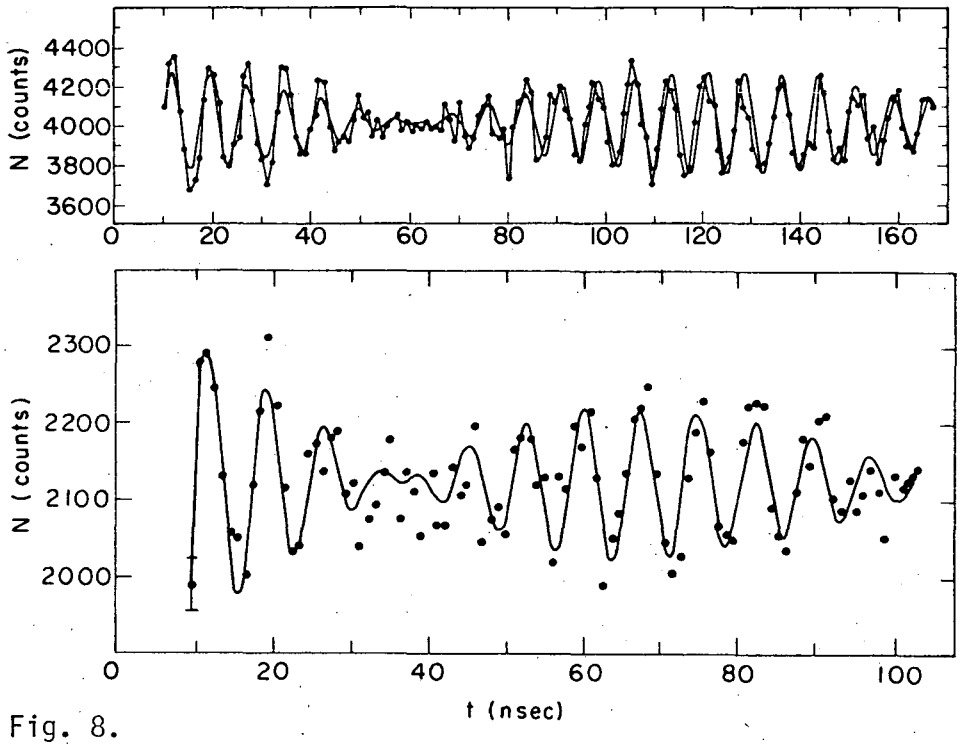

Fig. 8.

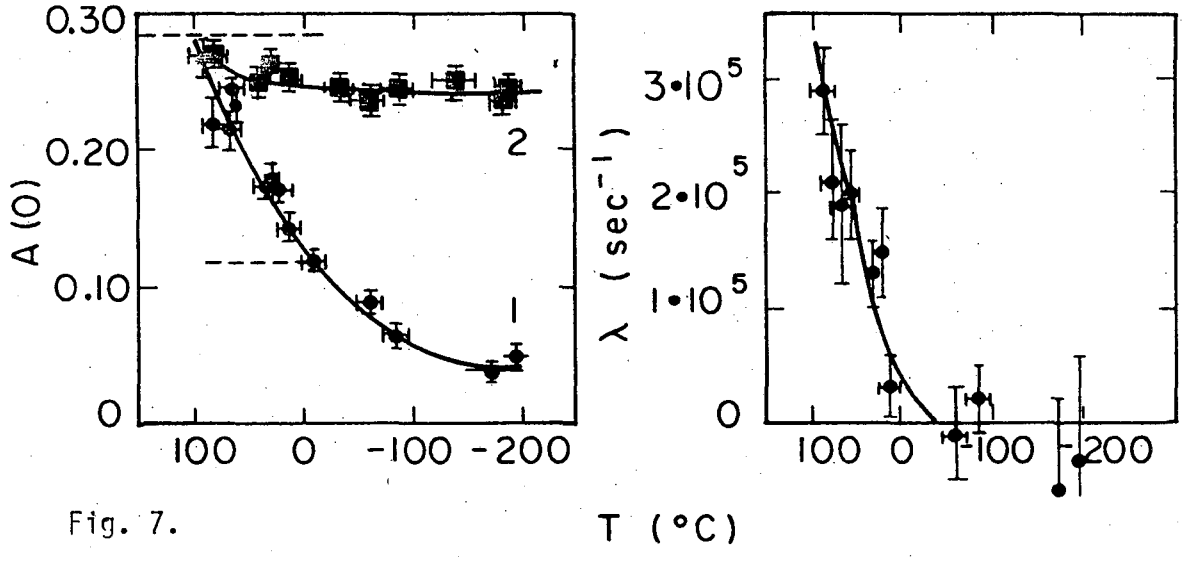

Fig. 7.

XBL741- 2144A

Fig. 7. Plot of μ^+ asymmetry as a function of temperature in Ge (left graph). The upper curve is for intrinsic Ge. The lower curve is for p-type Ge. The right hand graph is a plot of $1/\tau_2$ A function of temperature for P-type Ge. Data taken from Andranov et al.[13]

Fig. 8. Histogram of data for P-type Ge from Guervich et al. The upper curve for P-type Ge and the lower is for intrinsic Ge.

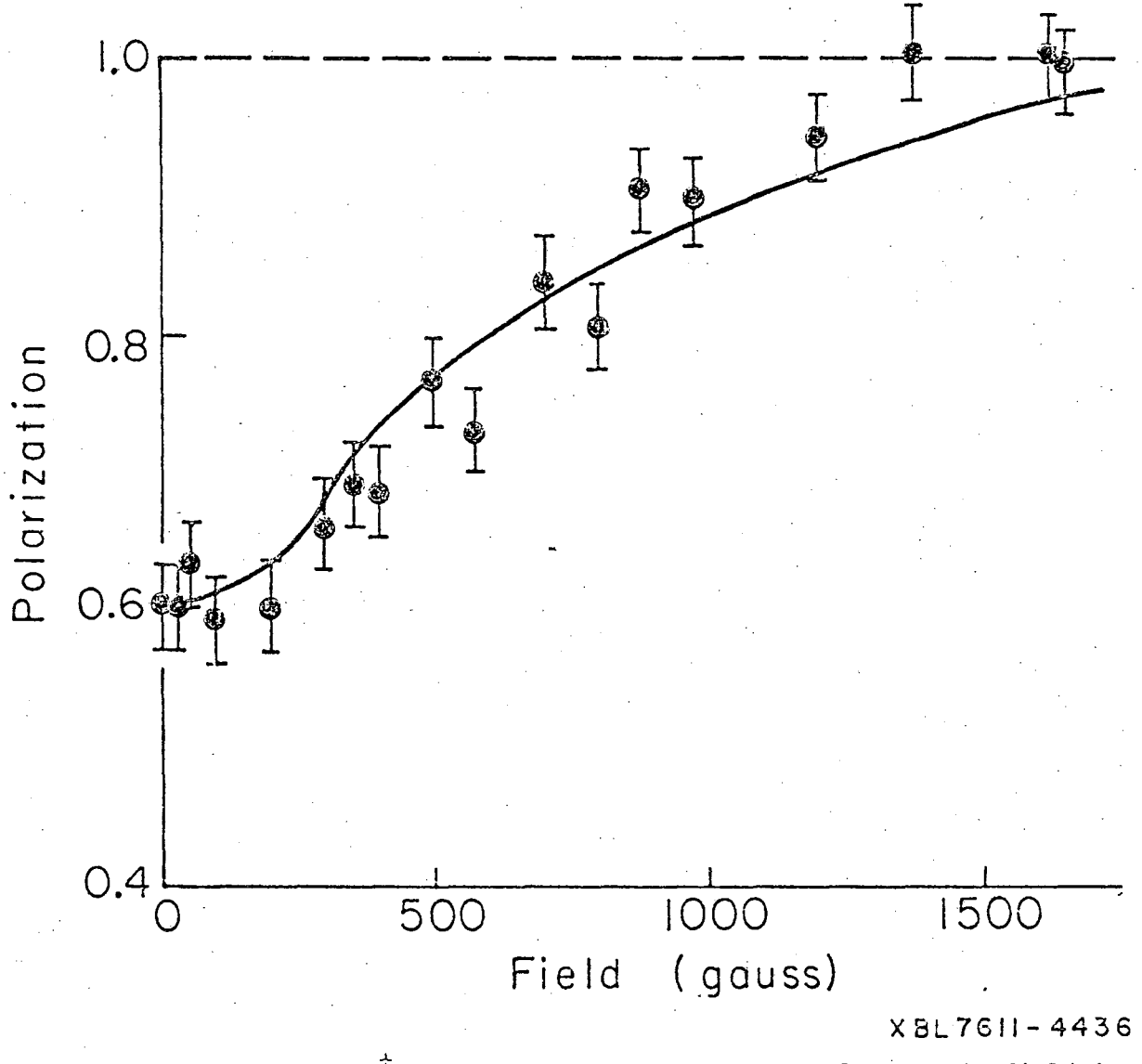

Fig. 9. Field dependence of the μ^+ polarization in a longitudinal magnetic field in a single crystal of silicon. Andrianov et al.[15]

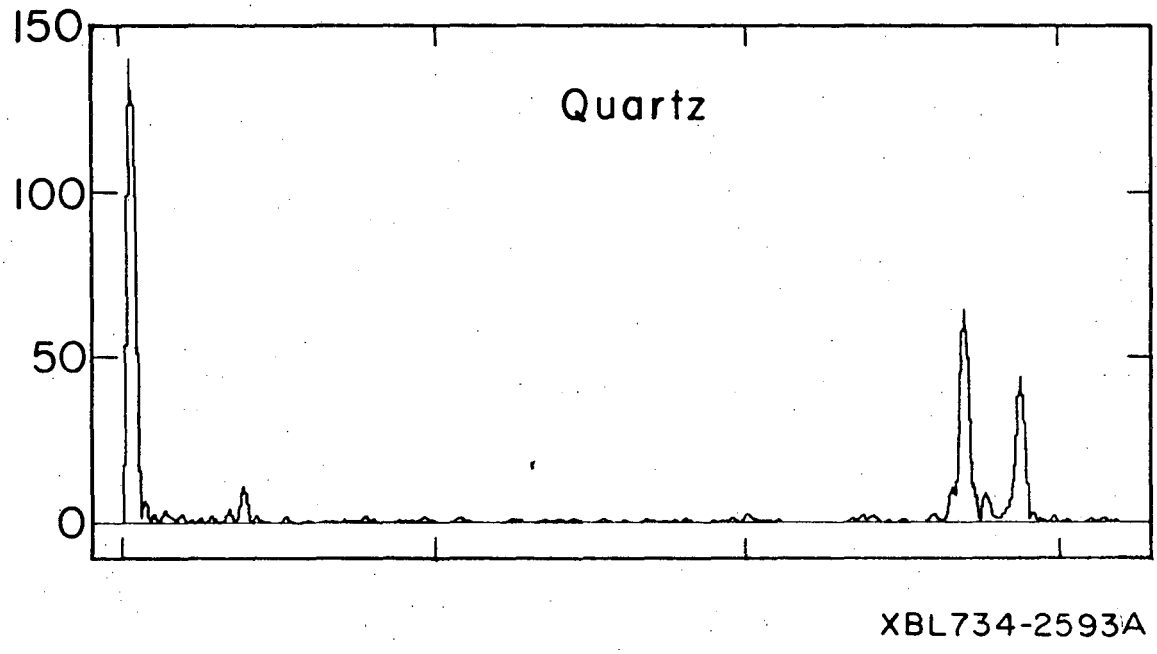

Fig. 10. Fourier transform of the power for quartz at 77°K. The two peaks near 150 MHz are the muonium precession frequencies. The lower frequency large peak is the μ^+ precession frequency.

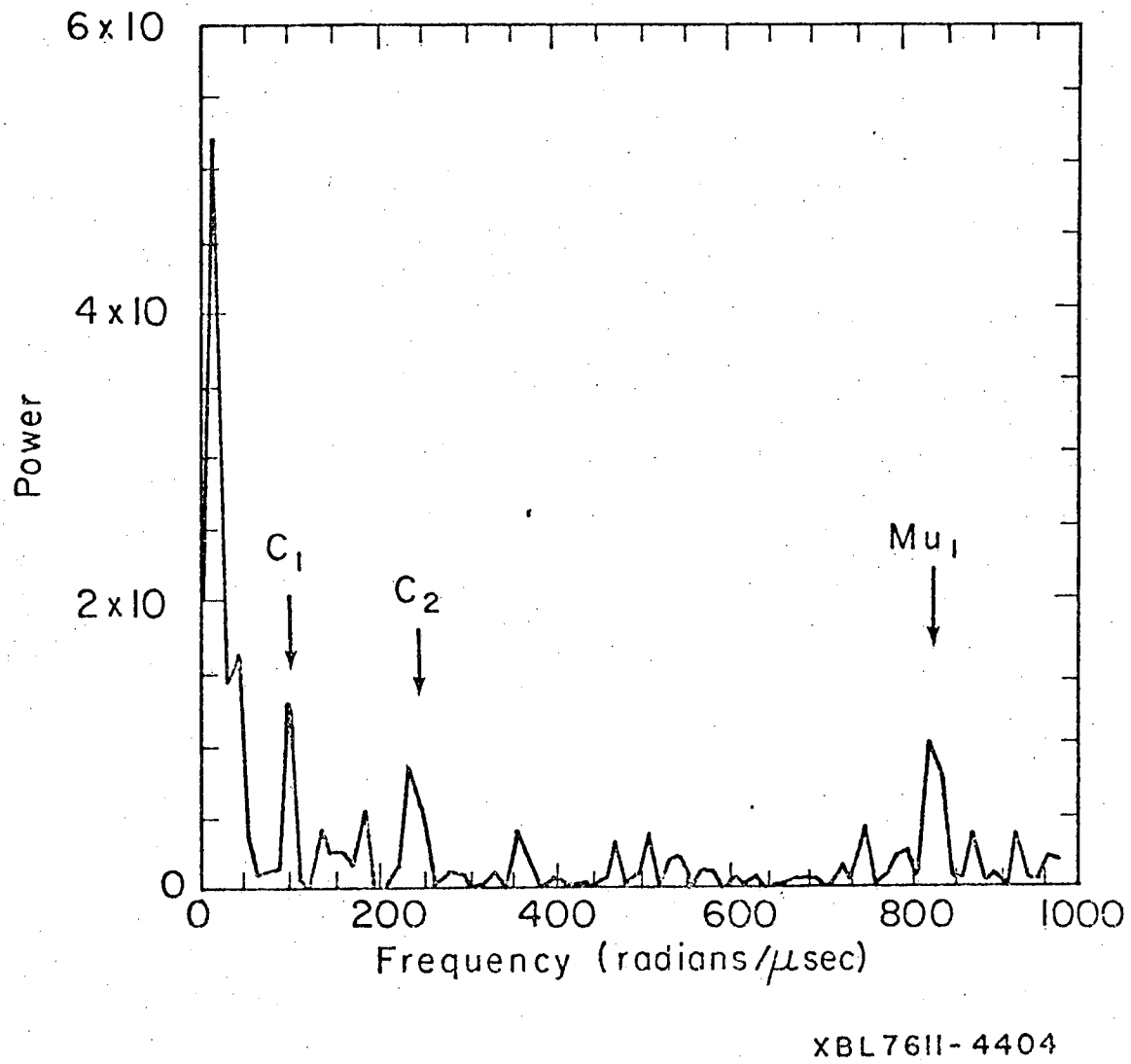

Fig. 11. Fourier transform of the power for p-Ge at 77°K. Where C_1 and C_2 are due to the rf structure of the 184 in. cyclotron at LBL. The highest frequency peak is the lower precession frequency of muonium. The largest peak is the muon precession (1.3 MHz). The frequency is in rad/μ-sec.

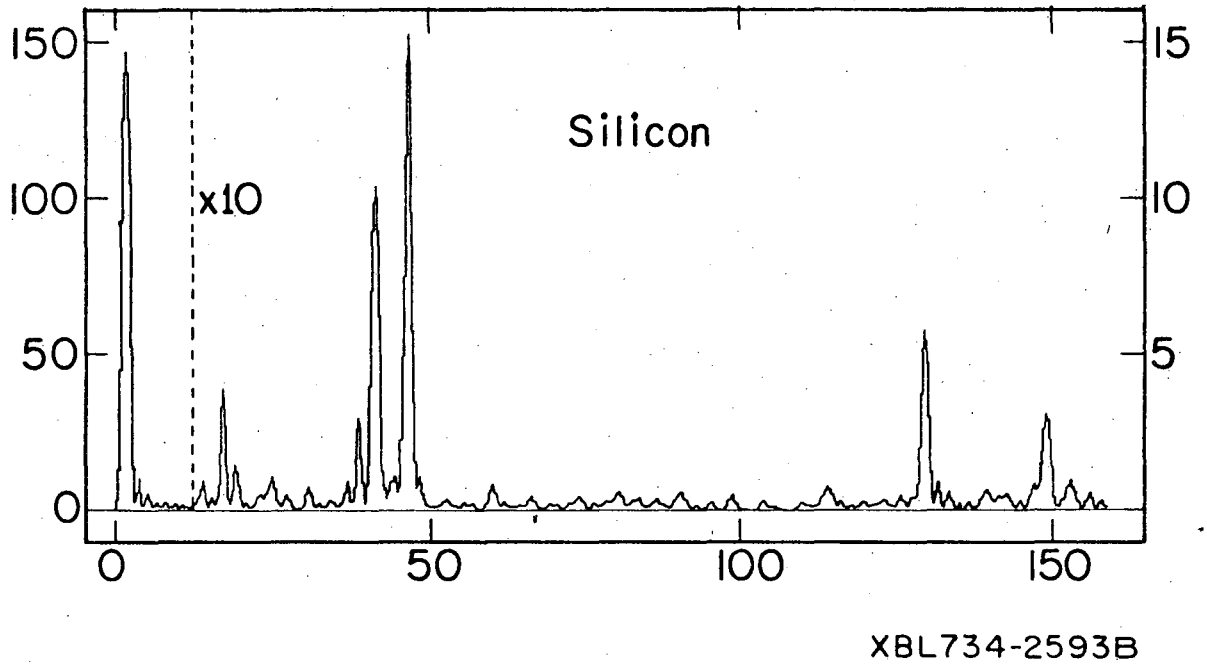

Fig. 12. Fourier transform of the power P_1-Si at 77°K. The two highest frequency peaks are due to muonium precession. The peak near zero MHz is the free-muon precession. There is also a series of peaks near 50 MHz; these have been designated anomalous frequencies.

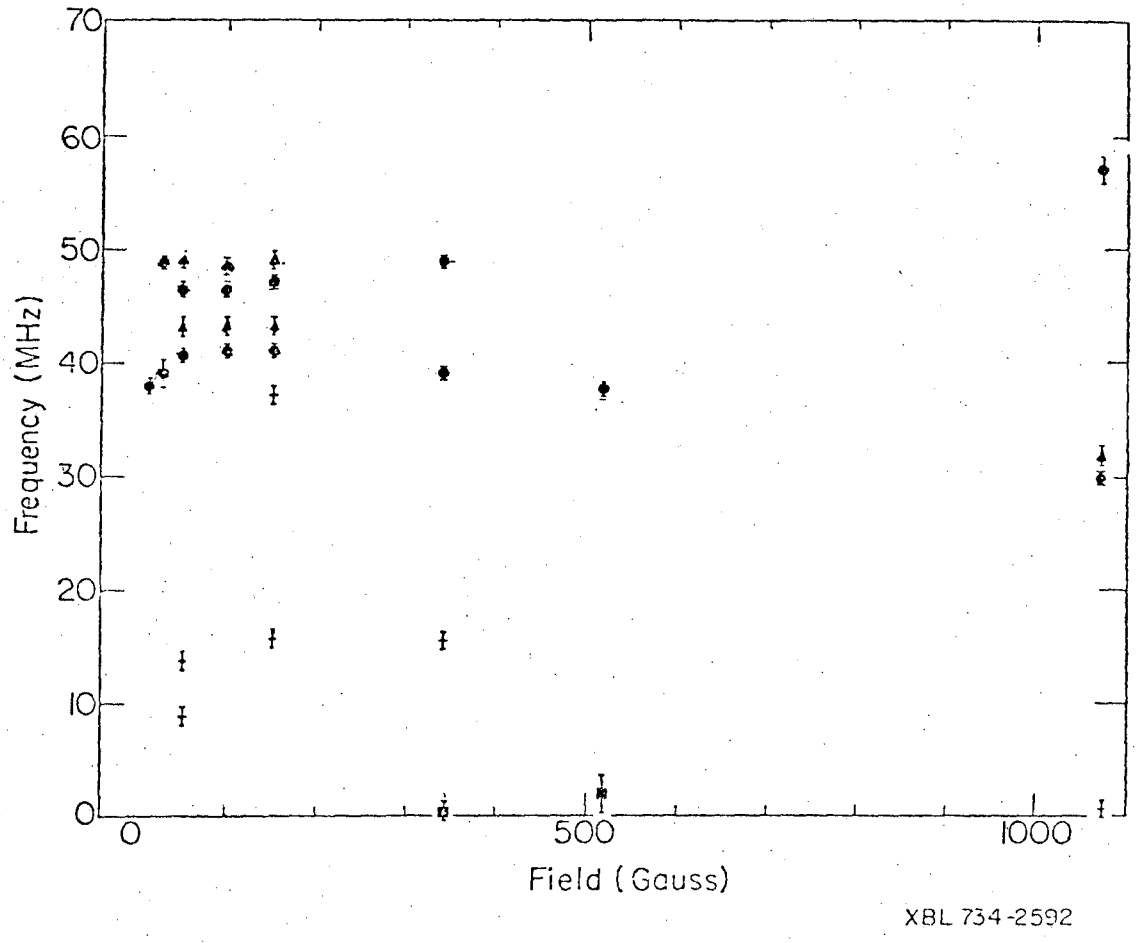

Fig. 13. Plot of the "anomalous" precession frequencies as a function of applied magnetic field. The displayed data is for the magnetic field along the [111] axis of the crystal (round points) and [100] axis (triangular points).

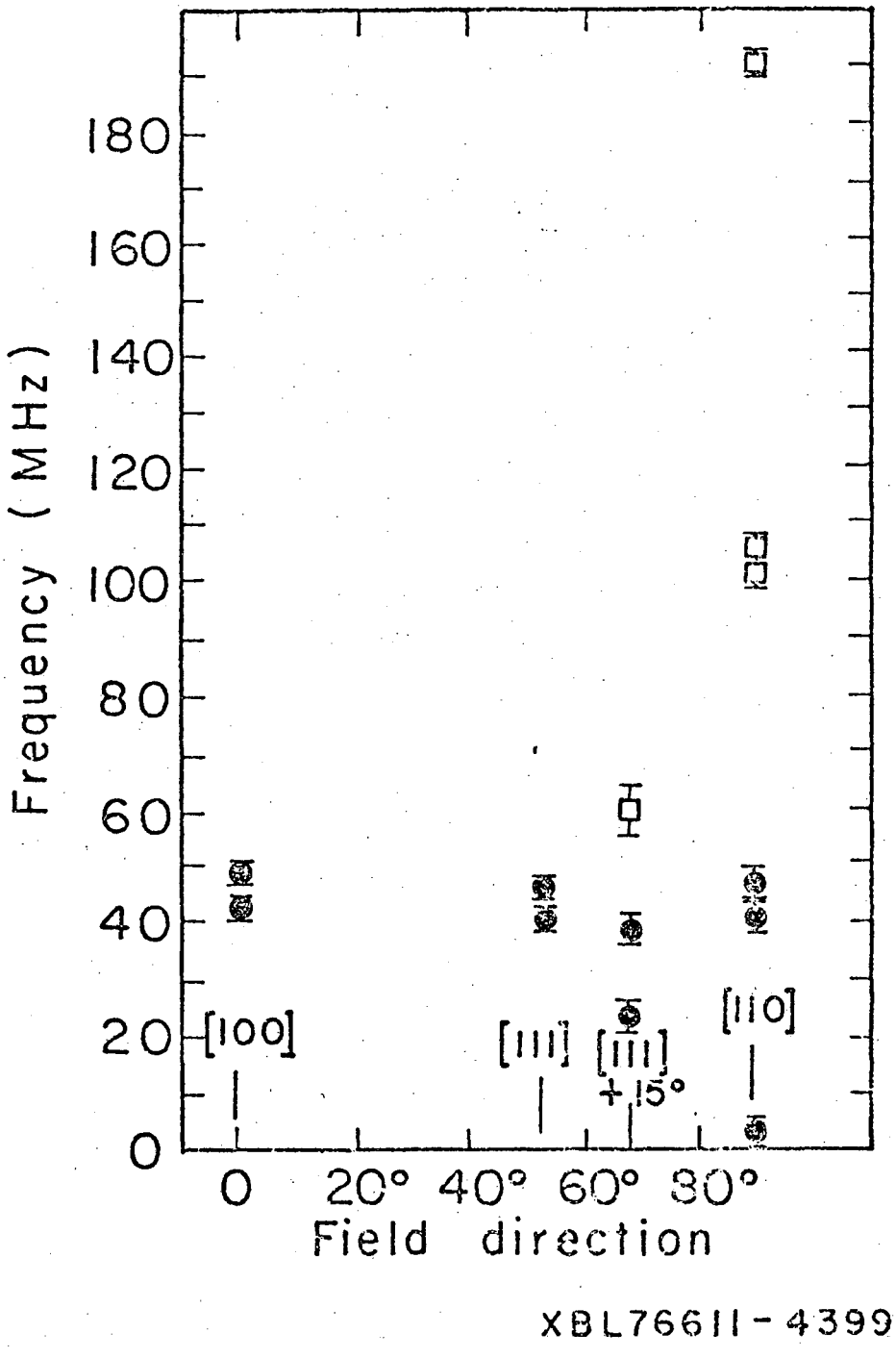

Fig. 14. Orientational dependence of anomalous frequencies as 100 G, 77°K in p-type Si.

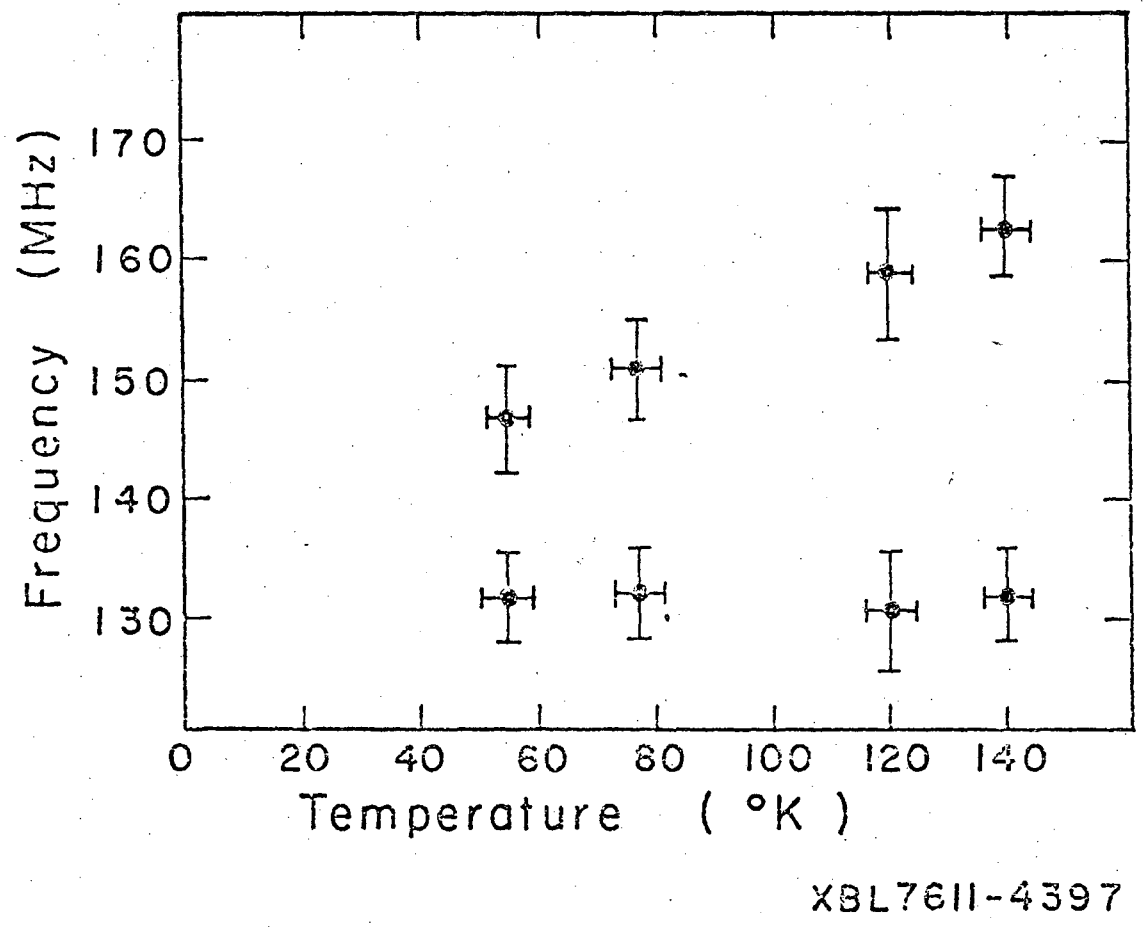

Fig. 15. Temperature dependence of muonium frequencies at 100 G. With the field along the [111] crystal direction. Included is the error due to the maximum drift in the magnetic field.

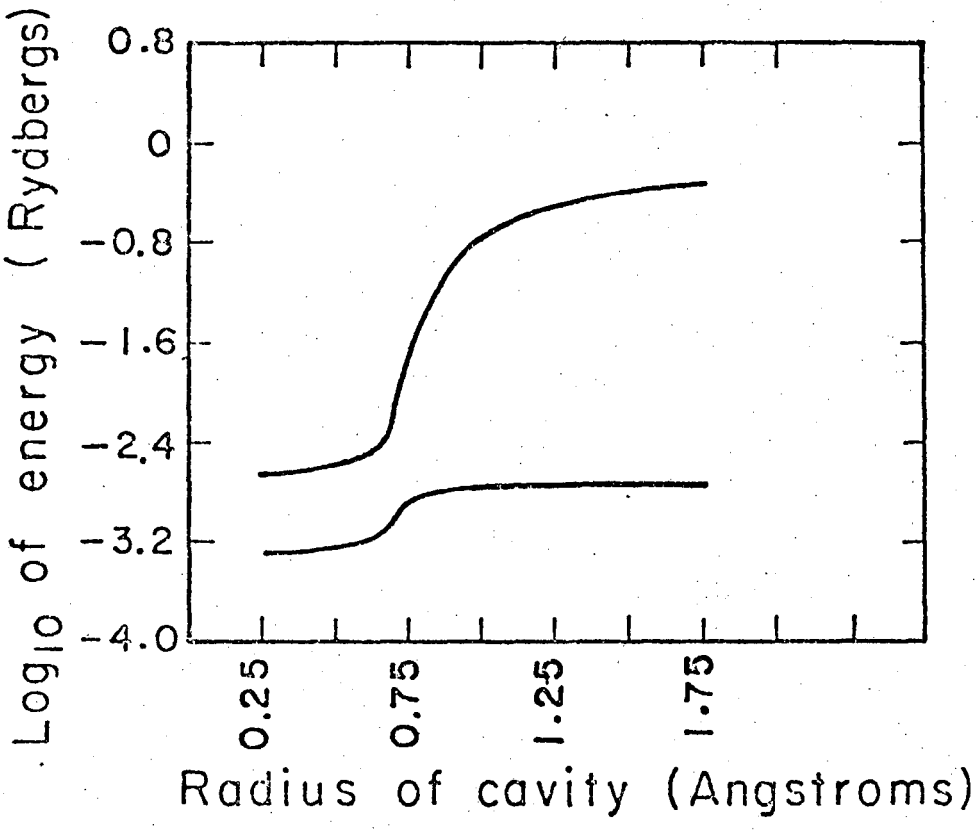

XBL 7611-4396

Fig. 16. Plot of the binding energy (in Rydbergs) as a function of cavity radius for the ground state (upper curve) and the first excited state (L = 1).

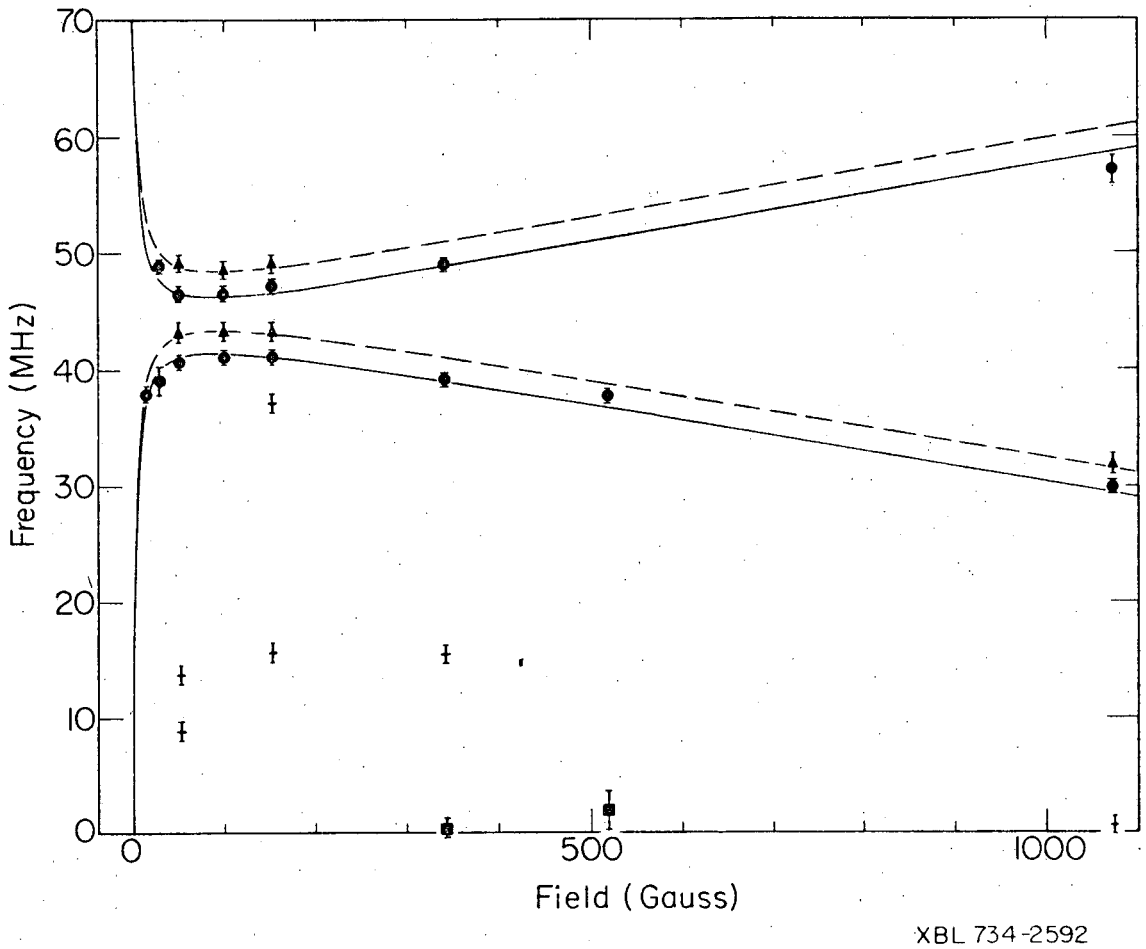

Fig. 17. Phenomenological fit of the anomalous frequency data for the [111] and [100] directions.

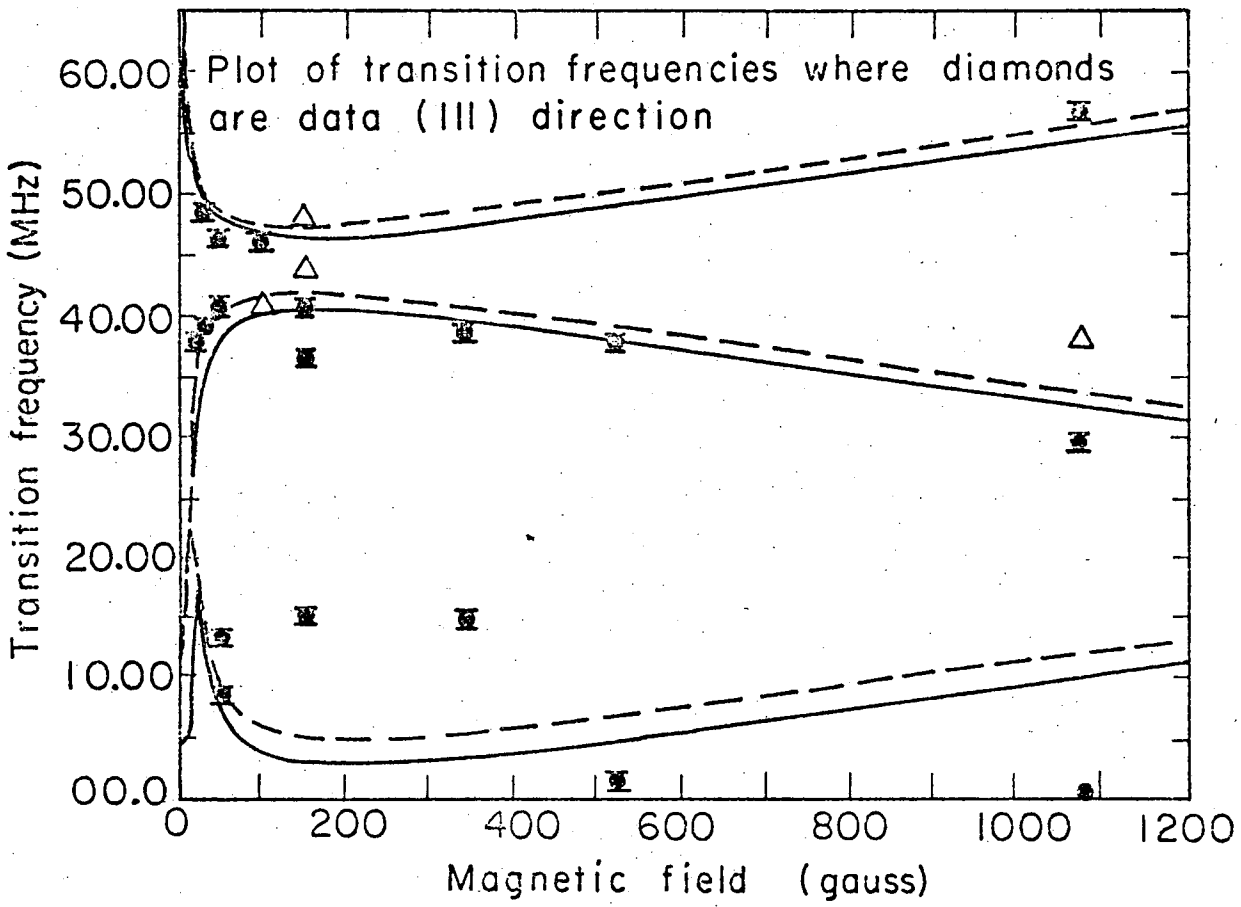

XBL7611-4403

Fig. 18. Fit of the anomalous frequency data where using the variational wave functions of Kohn and Littinger[11] for the [111] and [100] directions.

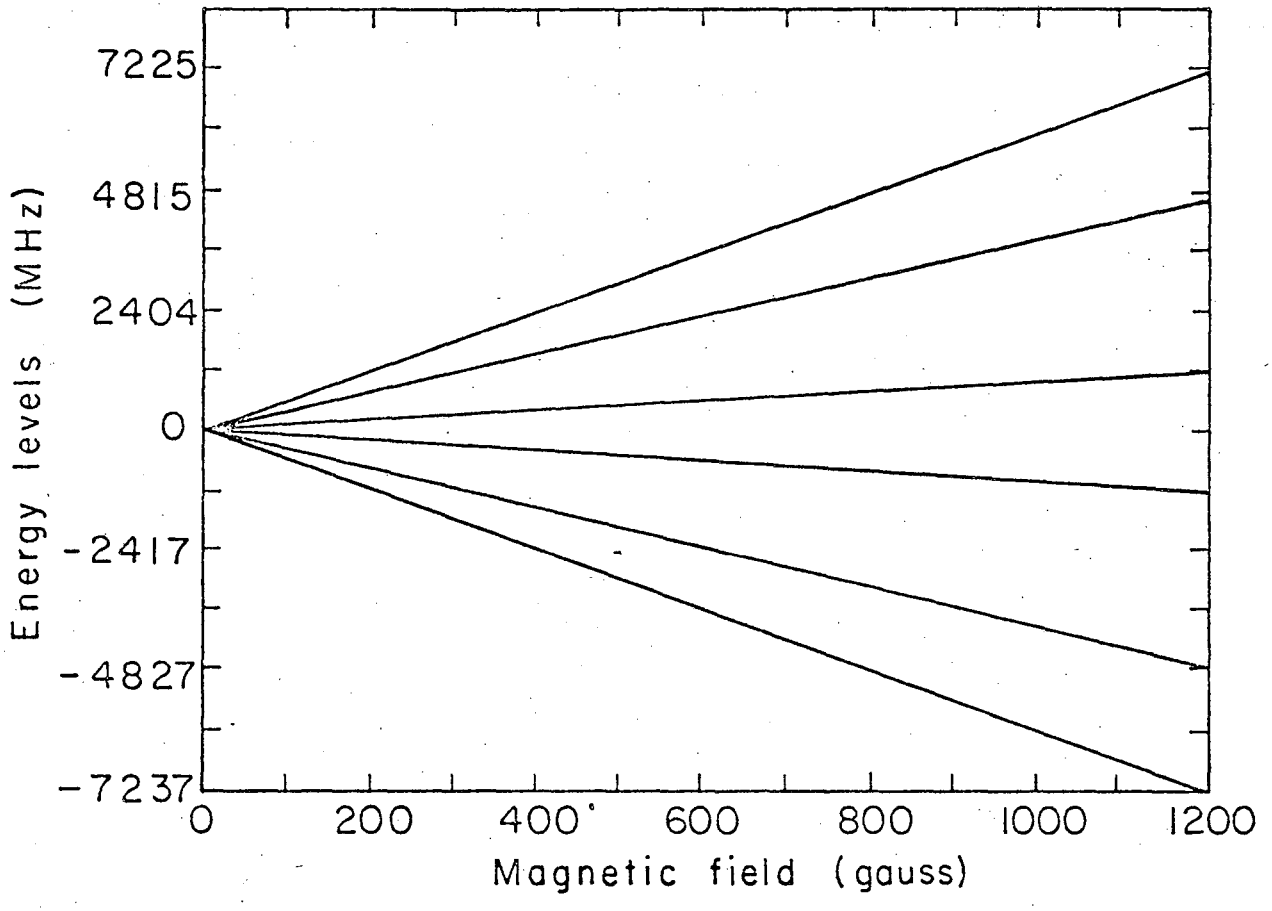

XBL7611-4398

Fig. 19. Plot of eigenstates obtained from the fit of the Tl state wave functions to the anomalous frequency data. Each one of the lines on the graph represents a doublet.

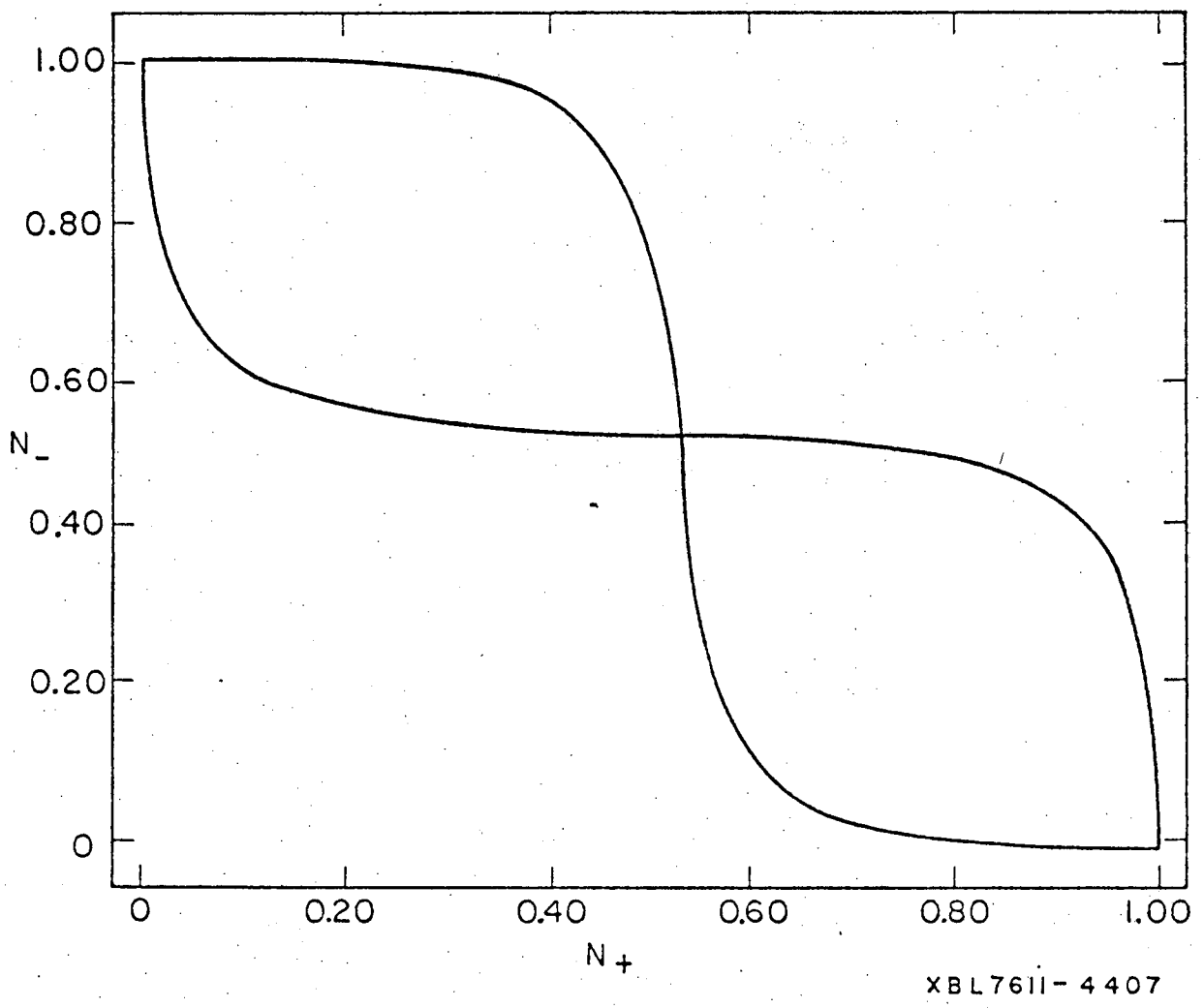

Fig. 20. Self-consistent plot of the number of spin up electrons vs the number of spin down electrons for a conductor with $U/\Delta \sim 5$.

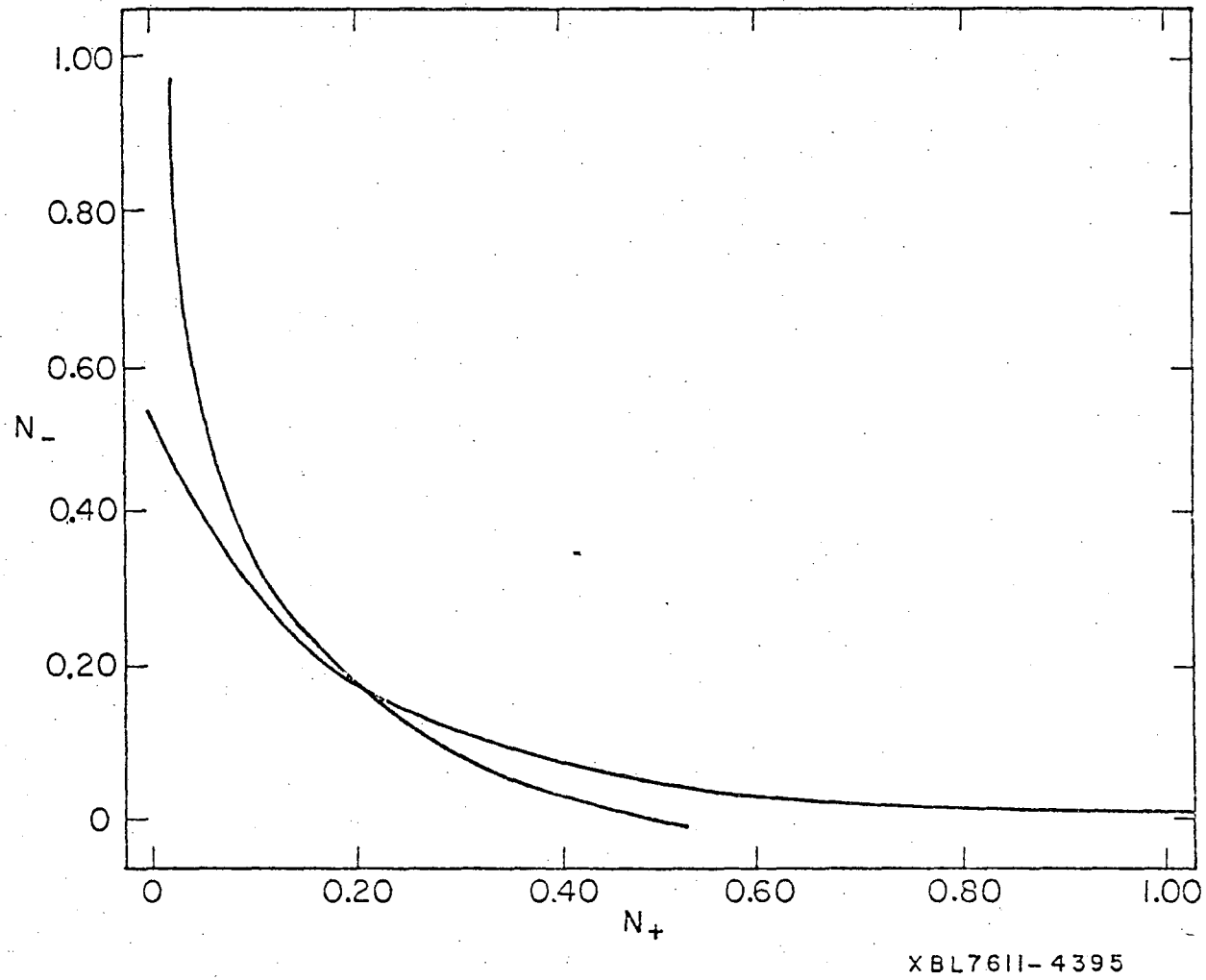

Fig. 21. Self-consistent plot of the mean number of spin up electrons vs the number of spin down electrons for a conductor with $U/\Delta \sim 1$.

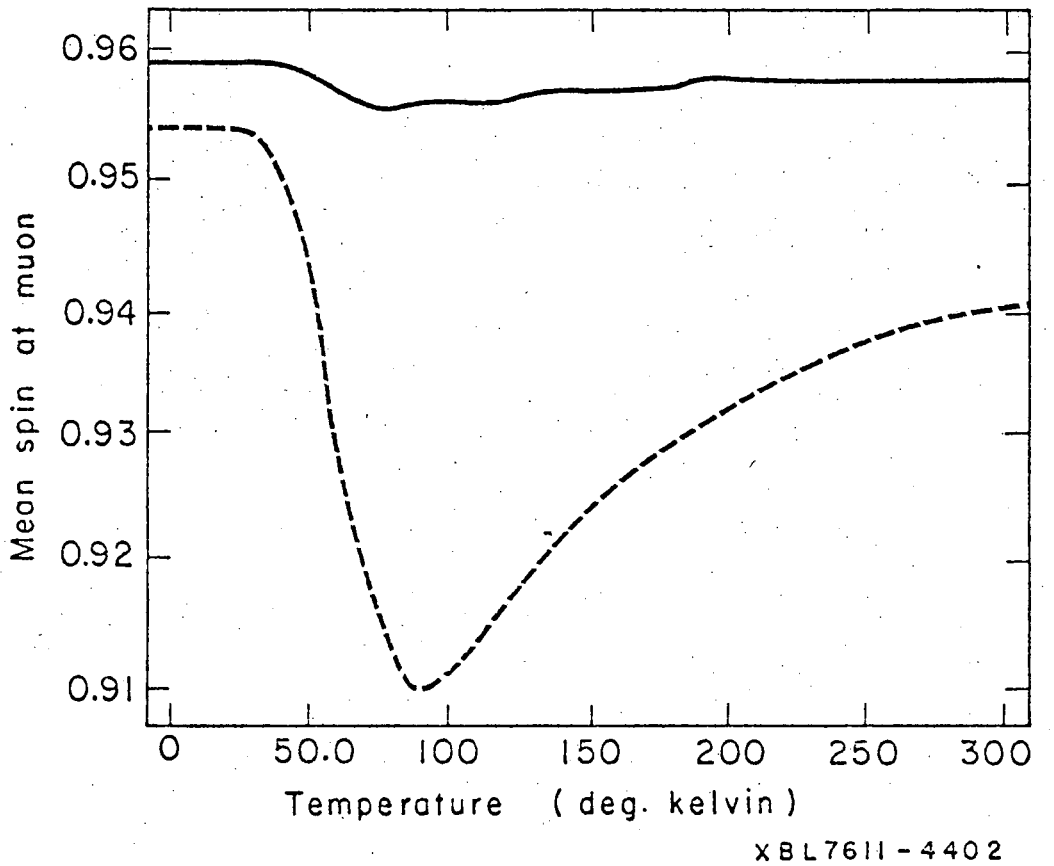

Fig. 22. Temperature variation of the net number of spin up electrons at the muon for a p-type Si sample which has a droping of 3×10^{14} B atoms/cm^3. Curve A is calculated assuming no variation of the energy gap with temperature and curve B assumes a variation of the gap with temperature.

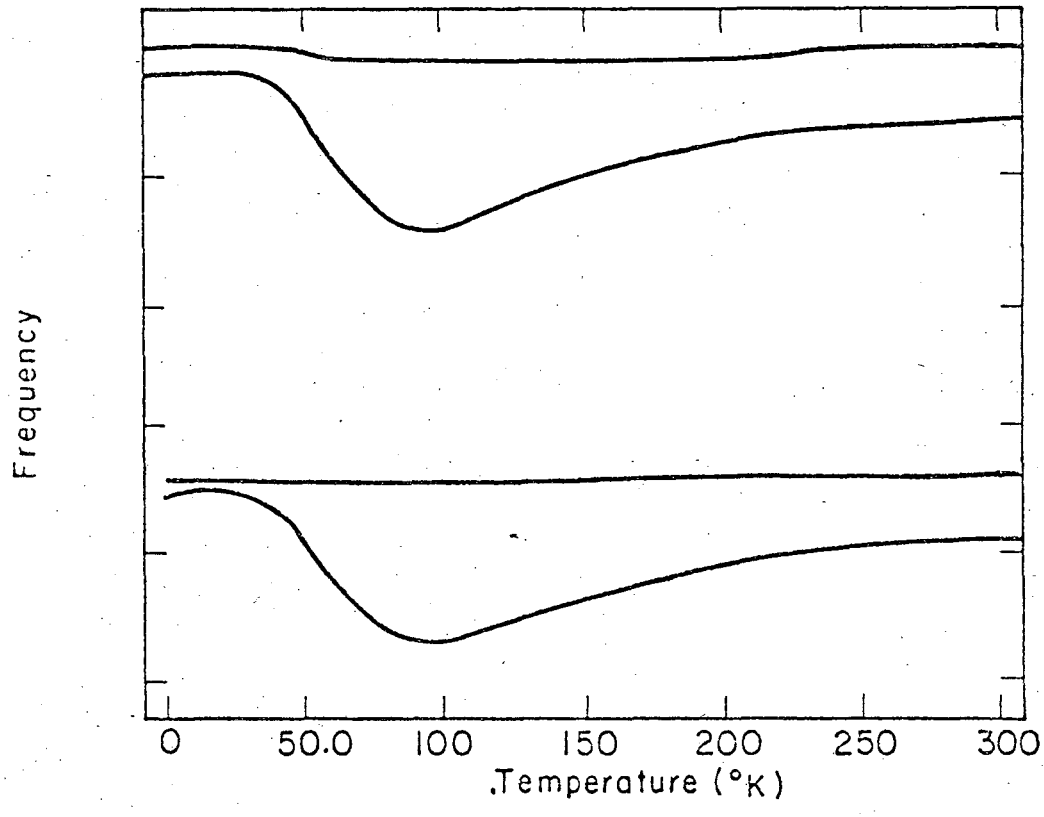

XBL7611-4401

Fig. 23. Plot of the muonium precession frequencies as a function of temperature assuming a localized moment. Curves A are calculated from the mean spins found without gap variation and curves B with gap variation. The doping is the same as that in Fig. 14.

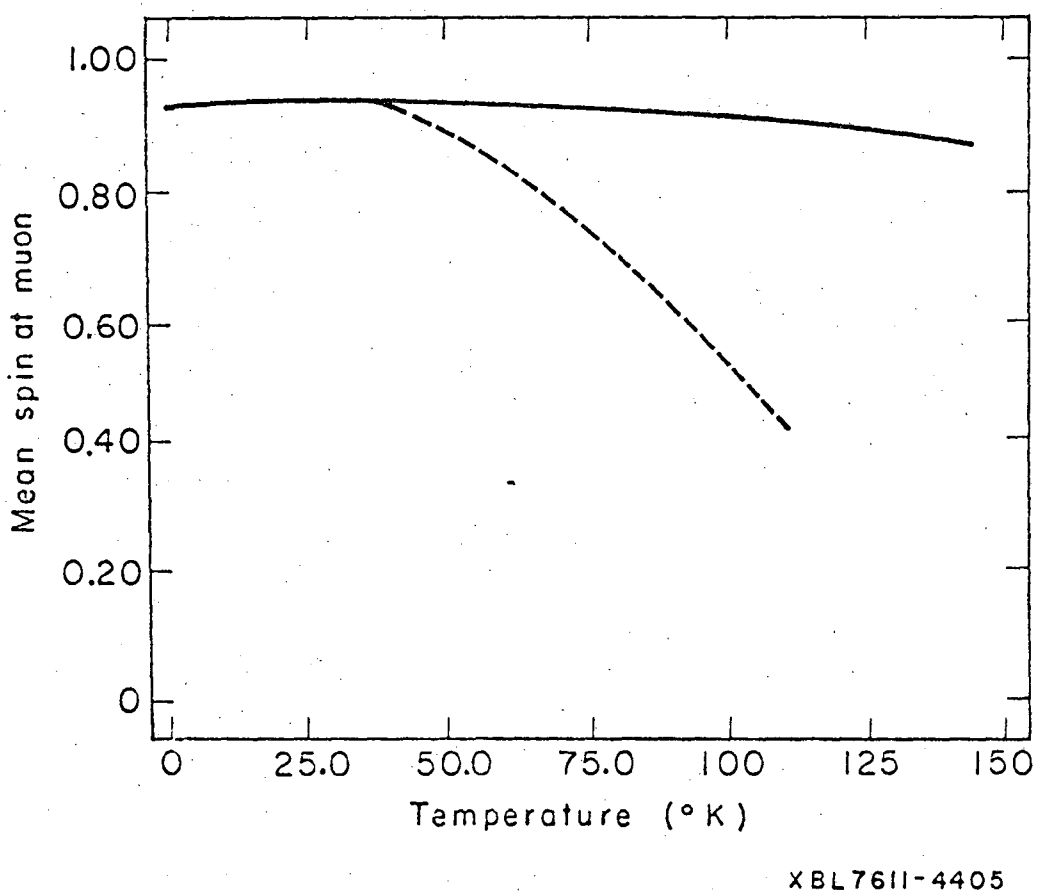

Fig. 24. Temperature variation of the net number of spin up electrons at the muon for a p-type Si sample which has a doping of 5×10^{18} B atoms/cm^3. Curve C is calculated assuming no variation of the energy gap with temperature and curve D assumes a variation of the gap with temperature.

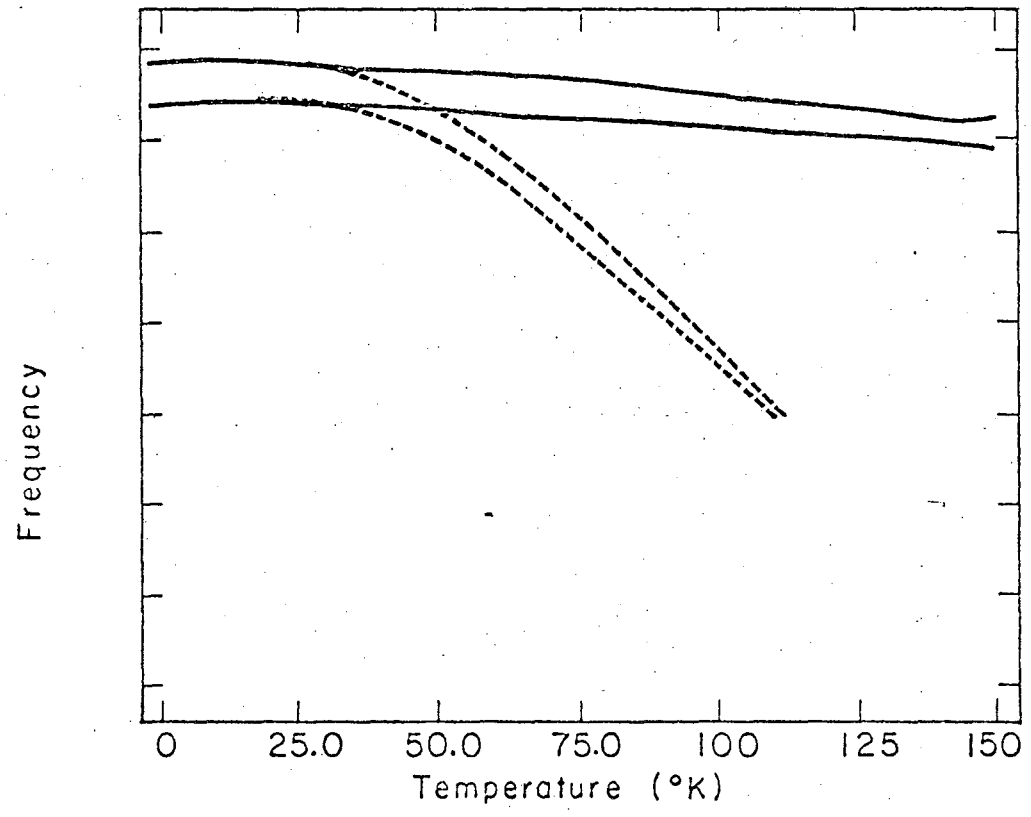

Fig. 25. Plot of the muonium precession frequencies as a function of temperature assuming a localized moment. Curves C are calculated from the mean spins found without gap variation and curves D with gap variation. The doping is the same as that in Fig. 16.

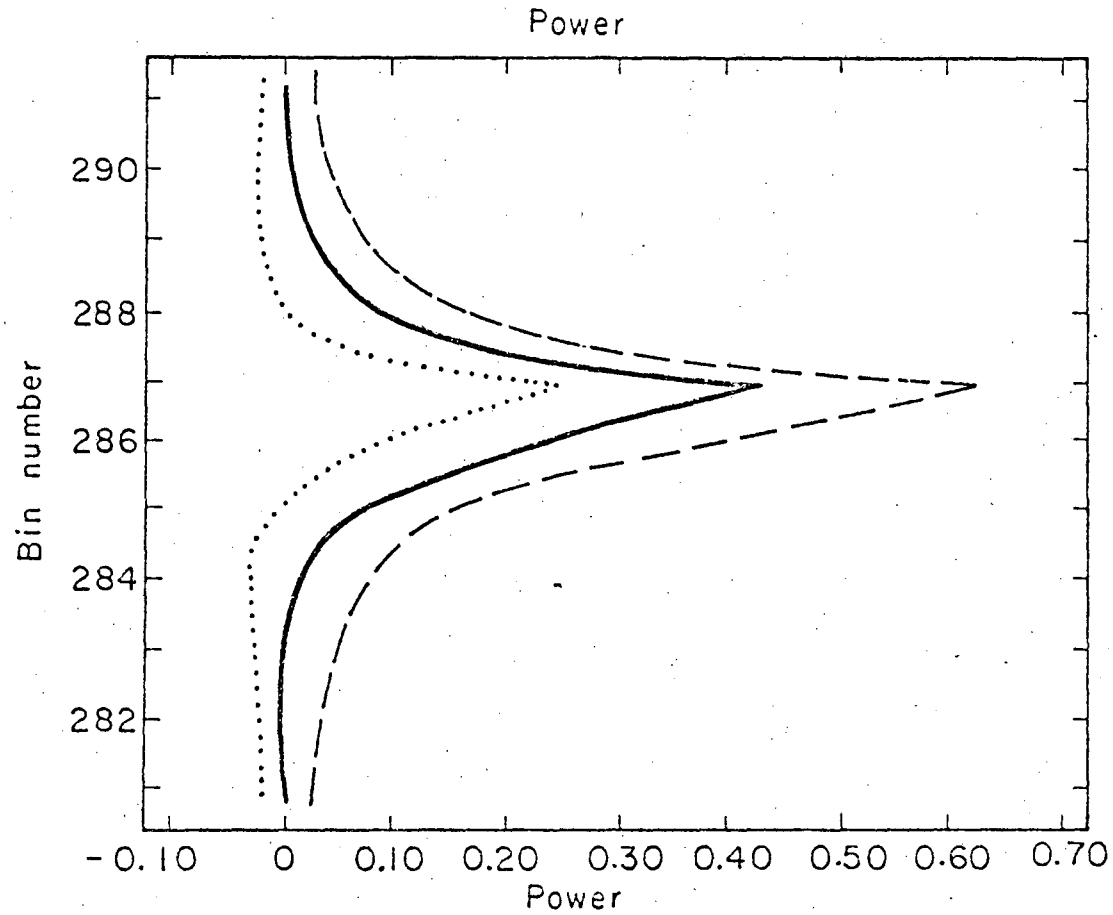

XBL 7611-4406

Fig. 26. Plot of signal power with error (±) for the lower muonium frequency peak in P_1-type Si at 77°K.

TECHNICAL INFORMATION DIVISION
LAWRENCE BERKELEY LABORATORY
UNIVERSITY OF CALIFORNIA
BERKELEY, CALIFORNIA 94720